2015

Dynamic Model of a Non-Linear Pneumatic Pressure Modulating Valve Using Bond Graphs

Christopher L. Brubaker
Cleveland State University

DYNAMIC MODEL OF A NON-LINEAR PNEUMATIC PRESSURE MODULATING VALVE USING BOND GRAPHS

CHRISTOPHER L. BRUBAKER

Bachelor of Science in Mechanical Engineering

Purdue University

West Lafayette, IN

May, 1994

submitted in partial fulfillment of requirements for the degree

MASTER OF SCIENCE IN MECHANICAL ENGINEERING

at the

CLEVELAND STATE UNIVERSITY

May, 2015

We hereby approve this thesis for
CHRISTOPHER L. BRUBAKER
Candidate for the Master of Science in Mechanical Engineering degree for the
Department of Mechanical Engineering
and the CLEVELAND STATE UNIVERSITY
College of Graduate Studies

Thesis Chairperson, Hanz Richter, Ph.D.

Department & Date

Jerzy T. Sawicki, Ph.D.

Department & Date

Jason Halloran, Ph.D.

Department & Date

Student's Date of Defense: April 30, 2015

ACKNOWLEDGMENTS

I would like to thank my thesis committee for their time and their help in substantially improving the quality of this work. Their questions, comments, and critiques were extremely helpful during the writing of this thesis. In particular I thank my teacher and advisor, Dr. Hanz Richter, for not only introducing me to these concepts and methods, but also guiding me through the research process.

I also would like to thank my wife Kellie for her support and sacrifice. I am especially grateful for the efforts she has taken with raising our son Benjamin who was born during the completion of this thesis. Without her help this work would not be possible.

DYNAMIC MODEL OF A NON-LINEAR PNEUMATIC PRESSURE MODULATING VALVE USING BOND GRAPHS

CHRISTOPHER L. BRUBAKER

ABSTRACT

This research develops a mathematical model of the dynamic pressure response to a variable travel input of a pneumatic pressure modulating valve intended for use in a vehicle air brake system. Generically, the valve is a multi-domain system consisting of a mechanical portion and a pneumatic portion. Included in the mechanical portion of the model are compliance of the springs, inertia of the components, and resistance of the sliding components. The pneumatic portion of the model includes capacitance due to the compressibility of the gas, flow resistance through connected plumbing, and flow resistance through the valve control orifices. The development of the mathematical model is accomplished using bond graphs and is complicated by the existence of several sources of non-linearities in the valve being modeled. The non-linearities are the results of mixed modes of operation, fluid dynamics of the gas, use of non-linear springs, and Coulomb friction. First, a bond graph is presented that accurately represents a linear version of the valve. Next the linear state derivative equations are derived. Next, the non-linearities are individually introduced by replacing those linear assumptions with actual, analytically derived non-linear equations and parameters are measured for inclusion in the model. Finally, the model is used to simulate the dynamic response of the valve using a simulation software package.

The simulated results are compared to experimental results and found to have good correlation. The model is suitable for use with simulation based design, or as a replacement for an actual valve in a Hardware In the Loop simulator of a vehicle braking system.

TABLE OF CONTENTS

LIST OF FIGURES

LIST OF TABLES

CHAPTER I

INTRODUCTION

This research develops a mathematical dynamic model for a pneumatic, continuously proportional pressure modulating valve using the bond graphs method. The type of valve modeled here is similar in design to that which might be typically used in a pneumatically braked vehicle to create a pneumatic control signal for delivery of a brake torque actuation pressure. Rather than providing a black box response based on system identification techniques and experimental measurement of the pressure response of the valve to a known input, this model is based on the analytic contribution of specific components contained within the assembly.

Often in a vehicle air brake system this type of valve is directly connected to the brake pedal and controlled by the operator's foot. It is referred to as a foot brake valve for this reason. The primary function of the foot brake valve is to instantaneously transform the operator's input (independent variable represented as plunger displacement) to a pneumatic control signal. Math models have been developed in industry which simulate or predict the characteristic response curve of the foot brake valve. These current, existing models of the foot brake valve are based on semi-static calculations [10] where a given input algebraically produces a desired pressure output from the foot brake valve. These models have been used in component design to determine spring and piston sizes, but have limitations when integrating

the valve component models with higher-level system models. Specifically, the pressure response of an actual valve is not an algebraic response to the drivers input, but rather a dynamic response. More accurately, the foot brake valve produces a mass or volumetric flow of air dependent on driver input, a supply reservoir pressure, valve characteristics, and feedback (in the form of output pressure) from the brake system. Pressure is then a dependent output of the integral of the resultant volumetric flow and system volume, compressed air properties, and gas temperature.

1.1 Motivation

It is desired to obtain an accurate model for a pneumatic proportioning valve which can be generalized, is modular in nature, and is easily simulated using standard engineering software packages such as Simulink and Matlab. A useful model will be easily integrated into a higher-level system model (such as a pneumatic brake system), and adaptable to changes in component parameters and even modifications in the valve design. Another desirable feature of the model is that it should be upgradeable. That is to say simplifications made within the current research may not be acceptable for all future applications or implementations of the model and users should be able to easily provide further detail when it becomes necessary. One method currently used to obtain models of the dynamic response for this type of pressure modulating valve is by experimentation where a prototype sample is built and the differential equation is obtained using system identification techniques [9]. More often, simulations are not obtained and elaborate physical systems are built in the laboratory and used for brake system testing and qualification. Experimental methods for modeling pressure modulating valves are effective for higher-level system design where an engineer has a set catalog of existing devices to achieve a desired system level output. Both methods described above require the manufacture of samples or prototypes and provide little

information about the inner workings and their effect on the behavior of the valve.

Prepackaged software has also been used to produce dynamic simulations of pneumatic pressure modulating valves analytically [17]. The prepackaged software method is more useful for product design than an experimental method because concept proposals can be evaluated quickly without the time and expense of prototype manufacture. Software packages complete much of the analysis for the engineer and can quickly produce a reasonable result for a trained user. The engineer however is limited to a set of predefined libraries which may not offer enough customization for the system under analysis and customization with prepackaged system modeling software comes at the cost of usability. The modeler may need to spend a significant amount of time simply acquiring the level of proficiency with the software needed to achieve the desired level of customization and simulation detail.

1.1.1 Application Opportunities

Modern pneumatic braking control systems are a combination of electronics and pneumatic valves. The electronics enhance a traditional, pneumatic-only system with improved vehicle stability (lateral stability, yaw, and roll control), reduced wheel slip during acceleration, reduced stopping distance, and other safety interventions. All newly manufactured pneumatically braked vehicles in North America have some level of electronic enhancement operating in conjunction with the vehicle operator and pneumatic control system. Although the final system effort is still a torque generated by the pneumatic/mechanical wheel end actuators, there are multiple pressure manipulations from a series of electronic valves and solenoids internal to the pneumatic control system. New electro-pneumatic valves are being developed to work within the higher-level mechatronic systems, and existing purely pneumatic devices are being used in applications and duty cycles for which they were not originally intended. These enhanced systems require the development of more sophisticated models in

order to efficiently design systems which meet the customer's needs. The dynamic response of the pneumatic and mechanical components of the system may not be as quick as is needed by the newer electronic controls. Relying too heavily on static or steady state response models of the component valves may create misleading results.

Existing dynamic models of the foot brake valve do not explicitly describe how internal components affect the dynamic response of the device. This limits the models usefulness in developing new products, or tuning products to meet specific characteristics that might be required by the overall vehicle system; particularly with respect to the response of the braking system to inputs from automatic, electronic control signal inputs. The design of a foot brake valve needs to consider not only how the nominal unit behaves with a nominal system, but also how it behaves when manufactured at the ends of tolerances, different operating conditions, and imperfect inputs. These considerations require a higher level of detail than is currently available about the components and their contributions to overall system dynamics.

Future higher-level system architectures have been proposed that will incorporate the use of an actuator and closed loop control system to apply the foot brake valve automatically. Concepts of devices that can automatically generate pressure signals based using closed loop control have been proposed [7] and [8]. A dynamic model of this proposed architecture, including the foot brake valve, will be useful during development and evaluation. It is necessary to verify the performance of a new type of architecture such as the one described above in all installations for all customers. Margolis cites several examples where modeling and simulation could have avoided costly mistakes when reapplying a known device or technology to a new application [13] and [12].

1.1.2 Current Work System Design

Air-brake system modeling using existing hardware and prototypes can be effective, but time consuming and costly. Model-based design is an alternative to creating physical prototypes for evaluating the dynamics of a proposed system. A limiting factor in moving to this type of model-based higher-level system design is the lack of available models of the control valves. Accurate dynamic models for valves of the type studied in this paper based on basic physical elements are not currently available. Dynamic models of pneumatic valves have added complexity due to their non-linear nature, inherent hysteresis, and compressibility of the fluid media. This added complexity makes existing predefined modeling software packages less than ideal for developing pneumatic system simulations.

The primary devices used in air brake control systems were developed in large part before the widespread implementation of electronic control enhancements in commercial vehicles such as antilock brake systems, vehicle stability systems, collision avoidance system, etc. The responsiveness of a system was only considered in the context of how quick the system was able to apply and release wheel-end torque and thus meet federal stopping distance requirements. Semi-static calculations were adequate for describing the behavior of the devices internal to the system.

Software prototypes offer advantages over physical prototypes in development time and cost. The commercial vehicle industry continues to place constantly increasing value on virtual, model based system design methods [18] over hardware-only methods. Of particular interest in higher-level system design is the transient response of the braking system to inputs from automatic, electronic control signal inputs. The primary devices used in air brake control systems were developed in large part before the widespread implementation of electronic control enhancements in commercial vehicles such as anti-lock brake systems, vehicle stability systems, collision avoidance system, etc. The responsiveness of a system was only considered in

the context of how quick the system was able to apply and release wheel-end torque and thus meet federal stopping distance requirements. Semi-static calculations were adequate for describing the behavior of the devices internal to the system and therefor dynamic models were not created.

1.2 Scope

This research develops a dynamic model of a pneumatic pressure modulating valve typically used in commercial vehicle air-brake control systems [11] using the bond graph method. The output of the physical valve is a volume flow rate at the delivery port in response to a variable pedal travel input and a constant supply pressure input. The model output in this paper is presented as a pressure as the gas flow fills a known volume. Figure 1.1 shows the physical boundaries of the system (valve) being modeled. This valve schematic shows the valve in the balance position with both the exhaust and inlet seats touching the rubber seal on the poppet. The poppet is in the neutral position with no compression of either the inlet or exhaust seal. Volumetric fluid flows and fluid pressure potentials are labeled.

Although the model in figure 1.1 shows a self-contained system, complete with supply pressure source and output volume, the intent of the model is to be coupled with upstream and downstream components in the higher level system. When coupled to these other components in a higher-level system model the physical system boundary is drawn to not include a source pressure and output pressure. The input is then the volumetric flow Q_{sup} and the output is the volumetric flow Q_{del}.

This research includes an accurate representation of the pressure output vs. plunger travel behavior of the valve by including in-depth analyses of energy storage elements, friction, and non-linearities within the valve. Also included within the scope of this research are experimental measurements of parameters and time

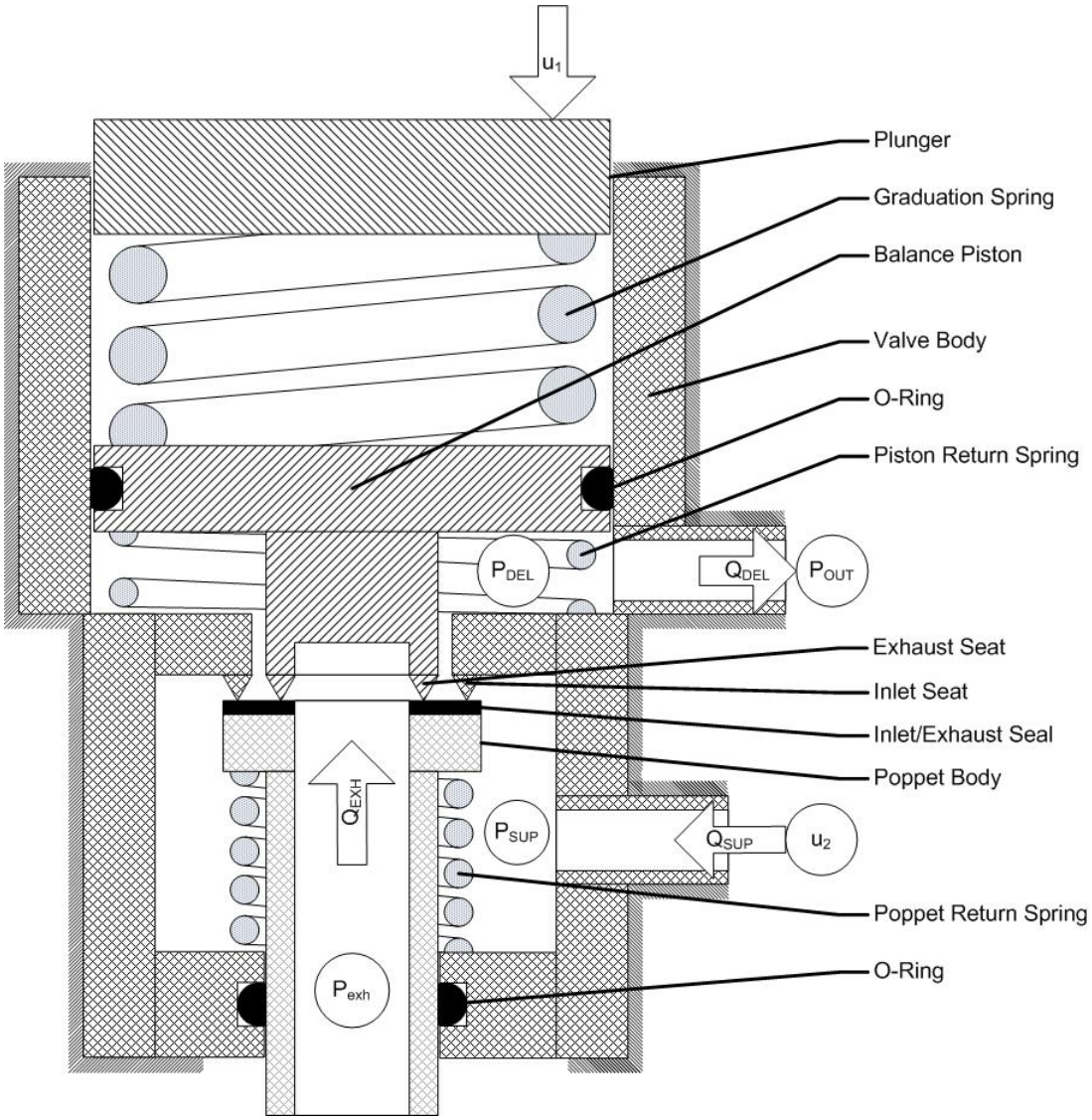

Figure 1.1: Valve Schematic

step simulations to various inputs. The results of the simulations are compared to experimental results of the actual system.

1.3 Bond Graphs

Keeping in mind the characteristics of the ideal model (accuracy, coupling with higher-level systems, and adaptability), the bond graph method was selected to find a mathematical model of the valve. The bond graph approach is an efficient method for obtaining a set of state differential equations for a system comprised of multiple energy domains [6]. In the case of this thesis there are two energy domains; mechanical translation and pneumatic.

The bond graph method offers a systematic way to develop a system model. There is a procedure for constructing the bond graph, a procedure for selecting the variables, and a procedure for deriving the equations. The state variables are automatically determined by the bond graph and a known number of first-order state derivative equations are obtained. The modular nature of bond graphs means that they can be easily coupled with other models to model higher-level systems. This modularity not only increases the utility of the bond graph for developing system models, but also makes the bond graph method easier to use than other methods. The system under investigation can be decomposed into smaller subsystems, bond graphs developed for those subsystems, and those subsystem bond graphs assembled to create the whole-system model. This method of model assembly can be simpler and more straightforward than drawing free body diagrams for each subsystem and solving a system of differential equations.

A great deal of insight regarding the nature of the system being modeled can be gained by studying the bond graph. While the resulting state derivative equations may be somewhat abstract to consider, the bond graph itself shows clearly the

conservation of power within the system. Energy loses can be thoroughly considered with the inclusion of energy dissipation elements. The individual contributions and interrelations of energy storage components are more easily understood than they are with other approaches; especially when the equations are manually formulated.

1.3.1 Construction

In a bond graph, 1-port energy storage and dissipation elements are connected through multiport junctions to form a subsystem. Those subsystems are then connected to each other in order to form a whole system. The basic construction elements are the same in the bond graph regardless of what energy domain is being represented. The elements are connected to each other with bonds which represent power. Each power bond has an effort e and a flow f. The effort and flow are selected such that their multiplication gives a result in terms of power for a true bond graph.

The bond graph has three energy storage or dissipation elements. These are referred to as basic 1-port elements and they are the resistance $-R$, compliance or capacitance $-C$, and inertia $-I$. A bond graph resistance is used to represent damping or friction in the mechanical domain, or flow resistance in the pneumatic domain. A bond graph $-C$ element is a spring in the mechanical domain and a fluid capacitance in the pneumatic energy domain. The inertia element is a mass in mechanical translation or a fluid inertia in fluid power.

There are also two 1-port source elements. They are the effort source $Se-$ and the flow source $Sf-$. In the mechanical domain the effort source would be a force while in fluid power it is a pressure. The flow source represents a velocity in mechanical translation and a volumetric flow Q in fluid power. Transducers are devices that instantaneously and ideally transform energy from one physical domain to another. There are two basic types of transducers in the bond graph; a gyrator $-GY-$ and a transformer $-TF-$. The transducer has two ports. One port may be

connected to a junction in the mechanical domain while the other port is connected by a power bond to the pneumatic domain. The transformer proportionately relates a flow on one side to a flow on the other side or an effort on one side to an effort on the other side via a modulus. An example of a transformer used in this thesis is the pneumatic piston. A fluid effort or pressure on the pneumatic side imposes a force on the mechanical side through the piston element $-TF-$.

The bond graph uses 3-port junctions to connect the various basic elements of the system and the 3-port junction may actually have any number of ports. There are two 3-port junctions; the 0-junction and the 1-junction. A 0-junction is used to connect elements all having the same effort. The 0-junction represents a common pressure in fluid power and a common force in mechanical translation. A 1-junction represents a common velocity in a mechanical system and a common volumetric flow in a fluid system.

An example system which can be conveniently modeled with bond graphs is shown in Figure 1.2. The example shows a system in two domains; mechanical translation and a pneumatic circuit. The basic physical elements considered in the mechanical domain are the mass inertia, viscous damping, and spring compliance. Similar physical elements are included in the pneumatic subsystem with the exception of inertia which is not included, and an effort source in the form of pressure is included. The mechanical subsystem is connected to the pneumatic subsystem via a piston actuator.

By inspection of the schematic it is determined that the compression velocity of the spring is equal to the compression velocity of the damper, and they are both equal to the velocity of the mass. These are considered equal flows in bond graph terms and they are all connected to a single 1-junction representing the velocity of the mass v_{mech}. The physics of the pneumatic subsystem are not as easily visualized. The pressure source generates a flow through a conduit and some pressure is lost to

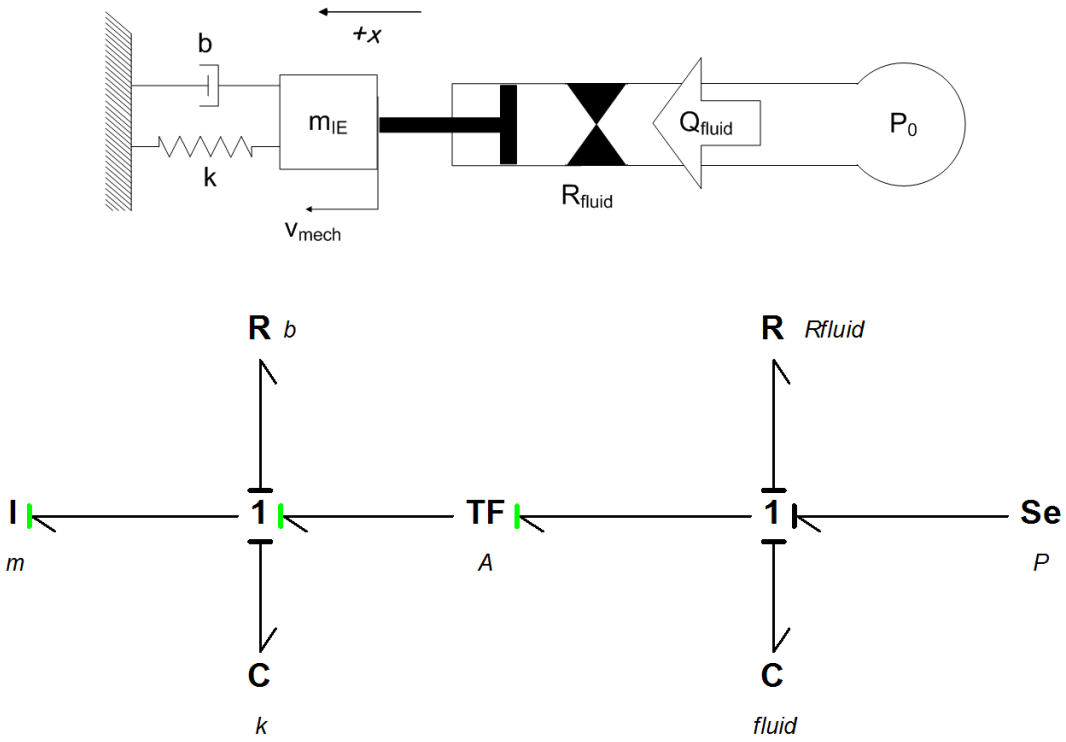

Figure 1.2: A Simple Bond Graph Example

fluid resistance and some is lost to fluid compliance. The volumetric flows for all three basic elements are equal so they are connected with a 1-junction representing the volumetric flow Q_{fluid}. The pneumatic circuit is similar to an electric circuit with voltage drops across a resistive element and a capacitor. The piston actuator is represented with a transformer in the bond graph with a modulus equal to the piston surface area A.

1.3.2 Causality and Through-Power

Each bond in the bond graph can either impose an effort or a flow upon the junction it is connected to. The convention is to add a hash known as a causal-stroke to the end of the bond where effort is forced. Causality is not arbitrarily decided, but rather rules and preferred forms are established. Some elements only make physical sense in one form of causality and hard rules are established by the bond graph

method. The effort source may only impose an effort and the flow source may only impose a flow. The effort source in Figure 1.2 is demonstrated to be imposing an effort by placing the causal-stroke away from the source element and next to the 1-junction. Transducers also have hard rules regarding the application of causal strokes that may not be violated. The pneumatic circuit in Figure 1.2 is imposing an effort in the form of pressure on the transformer which is in turn imposing an effort in the form of force on the mass. Flow may be imposed on a 1-junction by only one bond and effort may be imposed on a 0-junction by only one bond. Energy storage elements have a preferable integral form for causality, but the preferable form may be violated if the system dictates the use of the derivative form. Those instances where differential causality are necessary become apparent when inspecting the causality at the 1-junctions and 0-junctions. Dissipative elements do not have required or preferred causality form, but their causal assignments do have consequences with regard to the analysis of the bond graph. Causality is assigned to dissipative elements last and is often determined by which form is allowed by the rules governing the 1-junction or 0-junction to which they are attached. If the causal form is not determined for an energy dissipation element by the 1-junction or 0-junction it is an indication of an algebraic loop and special consideration during equation formulation will be required.

In addition to the causal stroke the bond also has a power half-arrow. Careful selection of the direction of the power half-arrow maintains sign agreement throughout model development. Some conventions are used to determine the directions of the arrows. Basic 1-port elements dissipate or store energy and the arrow points toward the element. Source elements provide energy and the arrow points away from the element. The engineer is required to use more judgment with arrow and power direction when connecting two 3-port junctions or with power direction in transducers. In these cases the engineer should consider the meaning of positive power and its effect on the system at the junction in question. The power arrow in the example in Figure

‘1.2 points away from the pneumatic circuit and into the transformer. The arrow on the mechanical side of the actuator points away from the transformer and toward the mass velocity. This selection indicates that a positive pressure on the pneumatic side will create a positive flow on the mechanical side.

Causality and through power are important in equation formulation. The state variables are determined by causality as well as the constitutive relations of the bonds. The sign conventions of the equations are determined by the direction of the power arrows.

1.4 Literature Review

Existing research was reviewed to determine what advancements have already been made in developing mathematical models and simulations of pneumatic pressure modulating valves. Application of the bond graph method to pneumatics was of particular interest. In addition to bond graphs and pneumatics, existing literature discussing nonlinear behaviors studied in this thesis were also reviewed. The bond graph method itself is accepted as established art and the primary bond graph reference used in this thesis is the text “System Dynamics: Modeling and Simulation of Mechatronic Systems” by Margolis, Karnopp, and Rosenberg [6]. Additional bond graph concepts by Das [5] and Borutzky [4] were also included. Compressed gas flow and valve behavior is described in many different references. The primary source of material in this thesis is Beater [2].

Accurate models of pneumatic pressure modulating valves have been created and used in the past such as that used by Hamdan to develop a modified PID controller [9]. However, that model does not provide detail internal to the valve. It treats the valve as a “black-box” where only the model response to a known input is determined. It is useful for system modeling and control system design where an existing valve

is used and objective is not optimization of valve performance, but not as useful for product design as a model derived analytically based on the internal components.

The type of valve considered in this thesis has been modeled previously analytically. Sridhar, Narayanan, and Kumaravel arrive at a dynamic response (apply time and release time) of a pneumatic foot brake valve used in a brake system using a software package and standard component libraries [19]. The authors do not identify the modeling software package used. Contributions of internal valve components are not described in detail. The simulation results appear to only be the product of a flow through an orifice equation and are not demonstrated in a true dynamic simulation. The concept of the bond graph technique is introduced in the paper as well as a description of how the pressure modulating valve functions, but those descriptions do not appear to be associated with the analysis or results. The authors do indicate that the selected software is based on the bond graph method. The model would be of limited use in a higher level system simulation because it is not shown that the model can be connected to a variable input in simulation.

A more rigorous application of software libraries used to produce dynamic simulations of pneumatic pressure modulating valves is presented by Peabody [17]. In Peabody's unpublished thesis she uses AMEsim software to develop simulations of multiple valves and assembles those models into a higher-level system. Prepackaged libraries within the software are modified and customized to the valves being analyzed. The work includes analysis of the nonlinear elements of the valves studied and specifically models the poppet sealing material as a combination of a linear spring and damper to achieve accurate results.

Many examples of specific applications of the bond graph method to pneumatic devices were found. A pneumatic gripper mechanism was modeled by Sakurai et al. using pseudo bond graphs for the pneumatic portions [20]. Zhu and Barth also apply pseudo bond graphs to pneumatics in the area of controls in [22]. Bera et

al. demonstrate application of the bond graph method to a V-twin engine comprised of thermal, pneumatic, and mechanical domains [3]. Those rigorous approaches all use a mass flow rate for fluid flow. The approach requires the use of pseudo bond graphs rather than true bond graphs because flow multiplied by effort does not result in power when mass flow rate is used selected for bond graph flow. This thesis uses volumetric flow as the bond graph fluid flow element and true bond graphs. Nonlinearities in the models described above are typically evaluated inside of the bond graph itself. The research in this thesis will handle case dependency and nonlinear elements outside of the bond graph inside of the simulation code.

Application of nonlinearities to the model is also of interest in this thesis; primarily friction and compressible gas flow. A survey of different friction models is presented by Olsson et. al. in [16]. The friction model used in this thesis was a modification of Coulomb friction to account for zero crossing in simulations without any consideration for stick/slip, but [16] does present the Karnopp model which is of interest as future work. The authors described the Karnopp model as useful in numeric simulation because of its inclusion of stick/slip behavior and ability to handle zero velocity.

1.5 Composition of Thesis

This thesis is structured in five chapters. The first chapter is the introduction and provides background regarding the system being modeled and the bond graph method used to derive the model. The second and third chapters develop the system model and simulation. The second chapter derives the system model as a set of state derivative equations using bond graphs as the basis. Nonlinear elements are identified in chapter 2, but constitutive equations are not derived. Specifics needed to simulate the valve system are derived in the third chapter such as nonlinear relationships and

initial conditions. Results of the simulations are provided in chapter 4. Chapter 5 is conclusions and future work.

CHAPTER II

SYSTEM MODEL

This chapter details the steps taken to develop the mathematical system model of the valve. While the bond graph was relatively straight forward, the non-linear nature of the valve presented some challenges for the analysis. For convenience the bond graph for the valve was developed as a linear system although it was previously determined to not in fact behave linearly. The assumption of linearity allowed the principal of superposition to be used for multiple input sources and the standard state space equation could be used to derive the set of state derivatives. A simple Simulink model could then be used to simulate the dynamics of the valve using the non-linear state derivative equations as the model for the valve.

2.1 Important Assumptions and Simplifications

The first step after establishing the boundary of the system which was defined in 1.2 is to determine what level of detail is necessary and sufficient to accurately describe the dynamic behavior of the valve in simulation. Assumptions and simplifications are made to reduce the complexity of the analysis.

1. Fluid flow can be modeled as simple flow through an orifice or pipe. In this study both the inlet orifice and exhaust orifice are modeled as flow resistance

and behave according to the familiar fluid power flow/pressure relationship for turbulent flow through a restriction [6]:

$$Q = A(t)\sqrt{\frac{2}{\rho}|P_1 - P_2|}sgn(P_1 - P_2) \tag{2.1}$$

Where P_1 is the upstream pressure, P_2 is the downstream pressure, $A(t)$ is the cross-sectional area of the orifice, and ρ is the fluid density. That simplification gives a satisfactory result for the purposes of this study. Further included in this simplification is an assumption of the geometry of the orifice. Whether the relationship is applied to the inlet or the exhaust, the shape is assumed to be the sidewall of a cylinder having a height equal to the clearance between the sealing material and seat, and a diameter equal to the diameter of the seat. This simplification is known to be incorrect in actual practice particularly when applied to the instances just before and just after either the seals open or close. It is known that in practice fluid will begin to flow while the rubber sealing material is still in contact with the seat. The orifice geometry will be such that the cross sectional area $A(t) = 0$ even though fluid will be able to flow with a pressure differential. The expected effect of this inaccuracy on the model is a decrease in sensitivity of the model when compared to the actual sample. The decreased sensitivity will be particularly noticeable as a hysteresis in the model which is higher than the physical sample.

2. Temperature and Supply Pressures are Constants. Repeated cycling of the valve will tend to increase the temperature of the gas and may deplete the supply source pressure. This model assumes that the gas temperature remains at standard temperature and is not heated by the action of the valve. Further, the input compressed gas source remains at a constant and known pressure and is not depleted or consumed by the action of the valve.

3. Valve May be Modeled Using Lumped Parameters. Variations along a length of tubing, across a surface, or throughout a volume are not considered in this analysis. All elements are considered uniform throught the element and be concentrated at a single point.

4. Pressure Changes are Small and Convected Internal Energy May be Neglected. The primary function of the valve is to direct the volumetric flow of the compressed gas into and out of a delivery chamber. It is not to compress the gas. Although it is known that the supply volume flowing through the valve must expand in order to achieve an increase in pressure at the delivery chamber, it is assumed that the work obtained by the volume expansion is negligible and the model would not benefit significantly with the added complexity required to account for the effects.

5. Fluid inertia in the pneumatic lines may be neglected. The one-port inertia parameter I for the two chambers internal to the valve, supply and delivery, are relatively small. The chambers are modeled as cylinders with large cross-sectional areas relative to their lengths. This geometry combined with the low density of the compressed gas all combine to create a negligible I value, so it is clear the fluid momentum may be neglected. This is not the case with the pneumatic lines into and out of the valve being modeled. Although the boundary of this system model is drawn around the valve only and does not specifically include the pneumatic lines, some physical parameters related to the pneumatic tubes are included in order to obtain normal behavior of the theoretical valve model as it would be experimentally tested. Both the supply and delivery ports in the model include a fluid resistance and a fluid capacitance related to the pneumatic tubes. They do not however include fluid inertia for reasons of simplification of the model. A stated requirement of the finished valve

model is for it be able to be coupled with other devices to form a higher level system. This coupling requires pneumatic lines which can often be long and with small cross section areas. The I values will be large and the resulting fluid momentum will also be larger and no longer negligible. The fluid inertia and momentum will need to be considered using a method such as that discussed by Margolis in "Bond Graph Fluid Line Models for Inclusion with Dynamic systems Simulations" [14].

These assumptions and simplifications are believed to be adequate for the purposes of obtaining a system dynamic response model of the valve. It is left as future work to complete in-depth studies into fluid inertia, friction, and fluid flow through an orifice as might be necessary for future applications of the model.

2.2 Physical System

A continuous pressure modulating valve of the type modeled in this research operates with two variable diameter flow orifices (inlet and exhaust) connected pneumatically to two separate volumes. One orifice is designated the inlet orifice and allows compressed air flow from the supply volume to the delivery volume. The exhaust orifice controls air flow from the delivery volume to the atmosphere. Increasing, decreasing, or steady pressure is achieved in the delivery volume by varying the net gas flow into or out of the valve. Higher mass flow out of the exhaust orifice than in through the inlet orifice will result in a decreasing delivery pressure. The opposite situation, inlet flow greater than exhaust flow, will result in an increasing delivery pressure. The orifice flow cross sectional areas are controlled automatically via a balance piston and springs. The operator sets the desired delivery pressure by varying the graduation spring force on top of the balance piston. The spring force is varied by increasing or decreasing the compression.

There are three operating modes for the valve. The first mode is exhaust open, inlet closed. The valve is typically in the inlet closed position during normal, zero fluid flow operation, but is also in this configuration during an exhaust event. The second condition is exhaust closed and inlet open which is typical of an application event. The final operating mode is the situation where both the inlet and exhaust orifices are closed. This condition is called the balance or lap position and is characterized by both the inlet and exhaust seats being in contact with the rubber sealing material. The valve will make a controlled apply (increasing delivery pressure) or release (decreasing delivery pressure) if either the inlet orifice or exhaust orifice are partially opened.

In order to model the modulating valve as a single system it is first decomposed into smaller subsystems and those subsystems are broken down into components. These smaller components correspond directly with one of the fundamental bond graph energy storage or dissipation elements. A mass corresponds with a bond graph [I] element, a spring corresponds with a bond graph capacitance [C] element, and a friction corresponds with a dissipative resistance [R] element when analyzing a purely mechanical system. The components are arranged into iconic subsystems in a way that accurately represents the valve. A mechanical velocity input representing the plunger travel is added to the primary piston subsystem and a reservoir pressure source is added to the fluid flow subsystem.

2.2.1 Balance Piston

The first sub-system is the balance piston and the boundaries for it include the piston itself, the exhaust seat, and the plunger travel input. Figure 2.1 shows how the pictorial schematic is redrawn as a lumped parameter schematic and eventually used to arrive at a bond graph of the subsystem. The various parameters affecting the function of the valve (mass, spring stiffness, friction) are included in

the diagram. As an intermediary step, the schematic diagram is further abstracted to show only indications of absolute velocity (1-ports) and forces (0-ports), and the appropriate fundamental bond graph elements (note that sliding friction is depicted as a viscous damper for simplification). Finally, the bond graph for the subsystem is drawn following the construction procedure outlined by Karnopp, Margolis, and Rosenberg for mechanical translation systems [6]. A 1-junction is assigned for each absolute velocity. Next the single mass in the subsystem is attached to the v_1 absolute velocity. A zero junction is connected between each absolute velocity and the appropriate subsystem elements are attached to those junctions. Note that at this stage of development all elements are assumed to be linear.

It is recognized during bond graph construction that the force F_7 acting on the mass is the result of a pneumatic pressure acting through a piston transformer. The other bond of the 2-port transformer is connected to a 0-junction representing the delivery pressure. This will be useful later when the pneumatic circuit is coupled with the mechanical translation subsystem bond graphs. Also, the zero velocity 1-junction can be removed at this point for simplification. Consequently the two 0-junctions connected to v_0 absolute velocity can also be removed and the 1-port elements attached to them moved directly to the v_1 1-junction. The result is as shown in the whole system bond graph in figure 2.4.

2.2.2 Inlet and Exhaust Poppet

The next sub-system analyzed is the inlet and exhaust poppet. Included inside the boundary of the poppet are the spring effects of the rubber coating which creates the inlet and exhaust seals, sliding friction, a mass, and a helical spring as shown in Figure 2.2. Similar to the balance piston subsystem the inlet and exhaust subsystem is redrawn with only the abstract lumped parameter elements, and is then annotated with absolute velocities and outside forces. The outside forces are

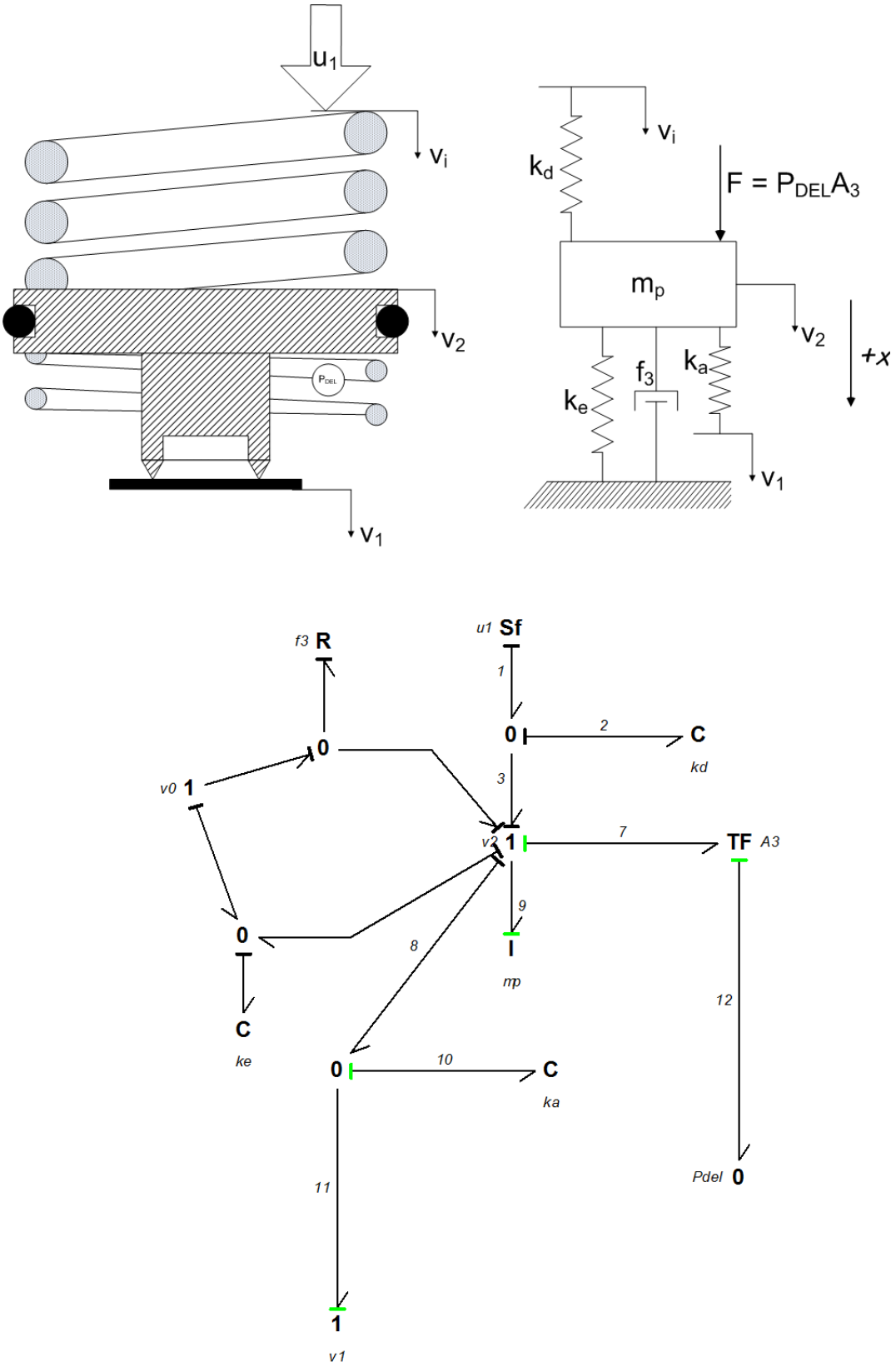

Figure 2.1: Bond Graph Development of the Balance Piston

recognized to be produced by piston transformers. Also, by inspection it is clear that absolute velocities from the previous balance piston sub-assembly are present in this poppet sub-assembly. They are depicted again in the bond graph for the subsystem. There are 2 springs connected to the 1-junction for velocity v_2; k_b for the spring effect of the rubber inlet seal and k_c for the helical return spring. These will be combined later into a single capacitive element in the system bond graph.

It is clear pictorially that the two forces due to air pressure act in opposite directions upon the mass. The delivery pressure acting on the A_2 area creates a positive displacement for a positive pressure, so the power half-arrow of bond 17 is drawn toward the 1-junction. The supply pressure acting on the A_3 creates a displacement in the negative x direction for positive pressure.

2.2.3 Pneumatic Circuit

The final subsystem modeled is in the fluid power energy domain. The bond graph construction for the pneumatic circuit subsystem is somewhat different from that of mechanical translation subsystems described previously. Assumptions and simplifications stated in section 2.1 are used to model the subsystem as a hydraulic circuit. The schematic is shown in figure 2.3 with each distinct absolute pressure. It should be noted that although absolute pressures are labeled here, gage pressure is used in all remaining models and simulations. The gage pressure P_{exh} is 0 psig. The schematic is then used to systematically develop the bond graph as detailed by Karnopp, Margolis, and Rosenberg [6]. A 0-junction is assigned to each absolute pressure. The absolute pressures are connected to 1-ports, and the variable diameter flow restrictions are connected to those 1-ports. Fluid capacitances for the chambers internal to the valve are connected to the 0-ports which represent the various internal pressures. Piston transformers are also connected to those 0-ports. These are the same transformers from the mechanical translation subsystems developed earlier. The

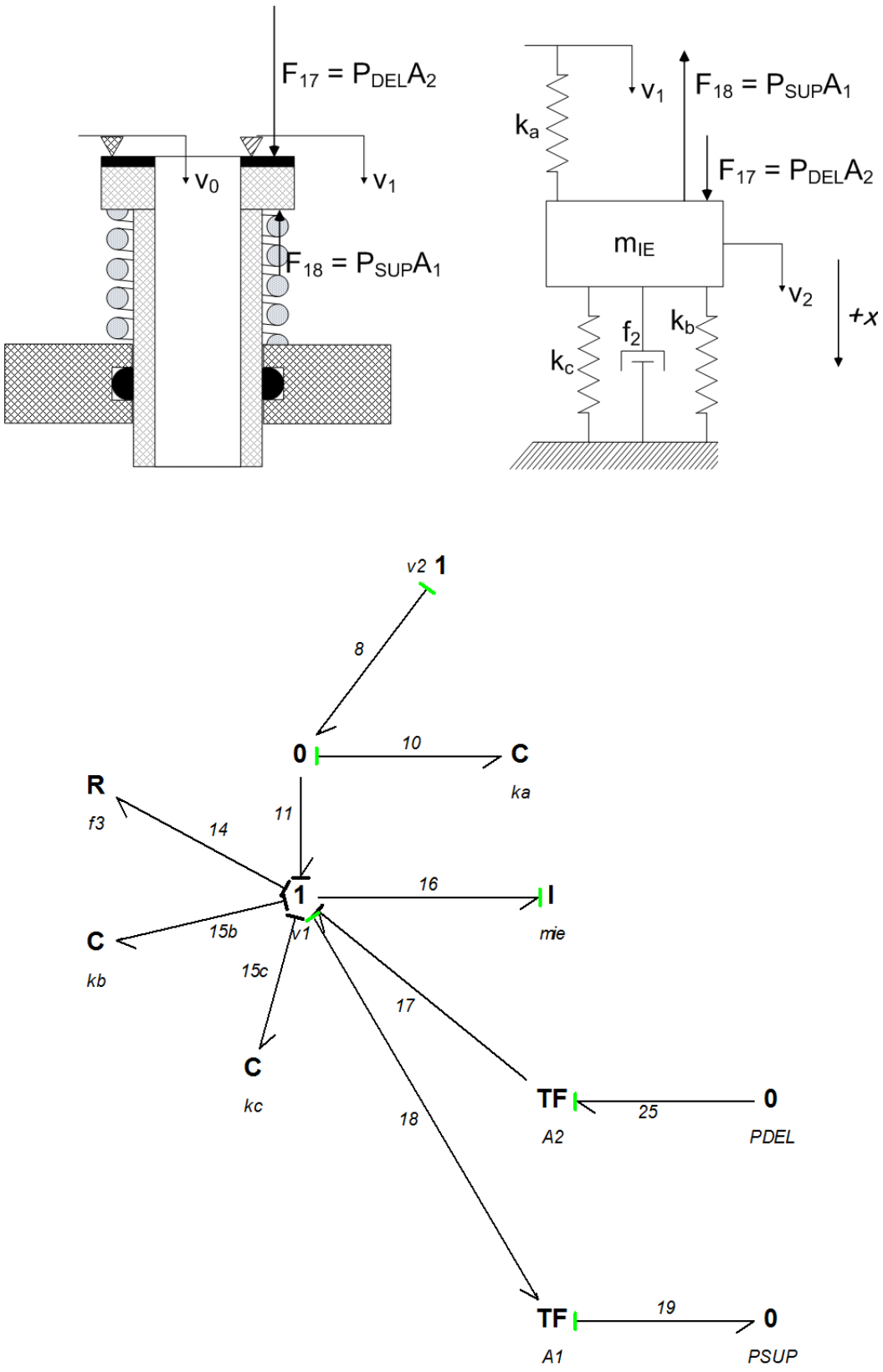

Figure 2.2: Bond Graph Development of the Inlet and Exhaust Poppet Subsystem

remaining 1-ports represent fluid flow through the pneumatic connections and linear, constant resistances as well as linear fluid capacitances are added to those 1-ports. The pressure effort source is finally connected to the 1-port representing flow into the valve to complete the subsystem bond graph. It is clear by inspection of both the schematic and the bond graph that the flow out (the valve output) is the sum of the two flows, less volume lost to the two pistons and capacitance, through the restrictions; Q_{sup} less flow volume stored in the capacitance and piston, and Q_{exh}. Flow through either restriction is designated to be positive if it flows in the direction of the delivery chamber. This means that flow out of the valve exhaust will be negative.

2.3 Bond Graph

It is clear by examination of the 3 subsystem bond graphs that each may be connected to the others through common 1-ports and transformers. Some simplifications are made such as removal of grounds (zero value efforts and flows) and elimination of 0-junctions and 1-junctions with only two ports and "through" sign convention. Causality is assigned based on integral causality for each energy storage 1-port element; C's and I's. Causality is then carried through using the rules of [1] and [0] 3-port junctions to power dissipating resistance R elements where possible. Inspection of the bond graph at this point shows that causality is automatically assigned to every bond. This leaves only power direction to be considered in augmenting the bond graph. Power direction is assigned to each 1-port element such that each power half-arrow is pointing into the element. Further the power direction for bonds 8, and 10 are assigned such that the spring is positive in compression. This leaves power direction to be somewhat arbitrarily decided for a few bonds. Careful consideration of the meaning of through power for each of the remaining bonds dictates a preferable direction for the remaining unassigned half-arrows. The half-arrows through

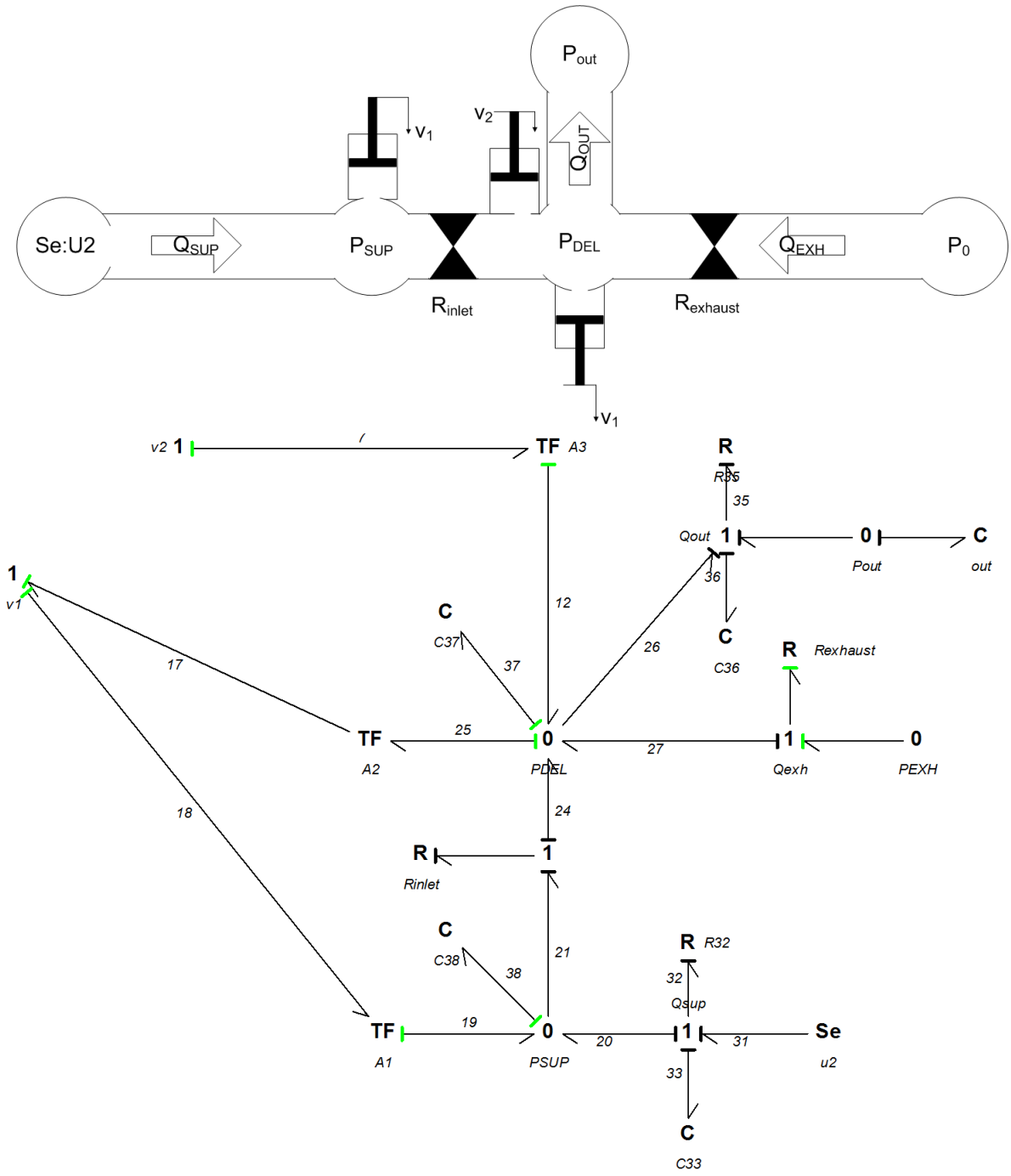

Figure 2.3: Pneumatic Circuit Subsystem Bond Graph

the transformers are drawn pointing into the pressure 0-junction for all cases. This means that a positive movement of the piston will create a positive pressure change when the transformer modulus is chosen as a positive number. The power half-arrow for the bond connecting the delivery pressure chamber in the valve and the output line/tank is drawn such that power flows positively in the direction out of the valve. During the simplification process the 0-junction representing the output pressure was removed and the vessel capacitance was combined with the pneumatic line capacitance. The output pressure in the simulations will be obtained from the effort caused by the remaining capacitive 1-port, C_{36}. The fully augmented bond graph is shown in figure 2.4. A great deal of information is provided by the bond graph. The resulting completed bond graph contains 2 independent inputs, 18 1-port elements, 10 independent states, 0 algebraic loops, and 0 elements with derivative causality. Although this bond graph provides sufficient information to begin the state derivative equation formulation, one further manipulation is completed to aid in the analysis. This final step in drawing the bond graph is to replace each of the non-linear resistance elements with a flow or effort source depending on causality. The sliding friction R_4 and R_{14} ports are effort causing elements and are therefor replaced with effort sources. The fluid flow restrictions R_{23} and R_{29} impose flow and are therefor replaced with flow sources. It is important to note that each of the 1-port elements being replaced is a resistance. Resistances do not add to, nor subtract from, the number of states provided causality is not assigned arbitrarily. This new, final bond graph is shown in figure 2.5.

This final bond graph with effort and flow sources substituted for the non-linear resistances is useful for automating the equation formulation process because it allows the application of linear analysis to a non-linear system. The new sources may be modeled as inputs. That means the principle of superposition may be used, and the 20-Sim [1] software may be used to analyze the bond graph as a linear system

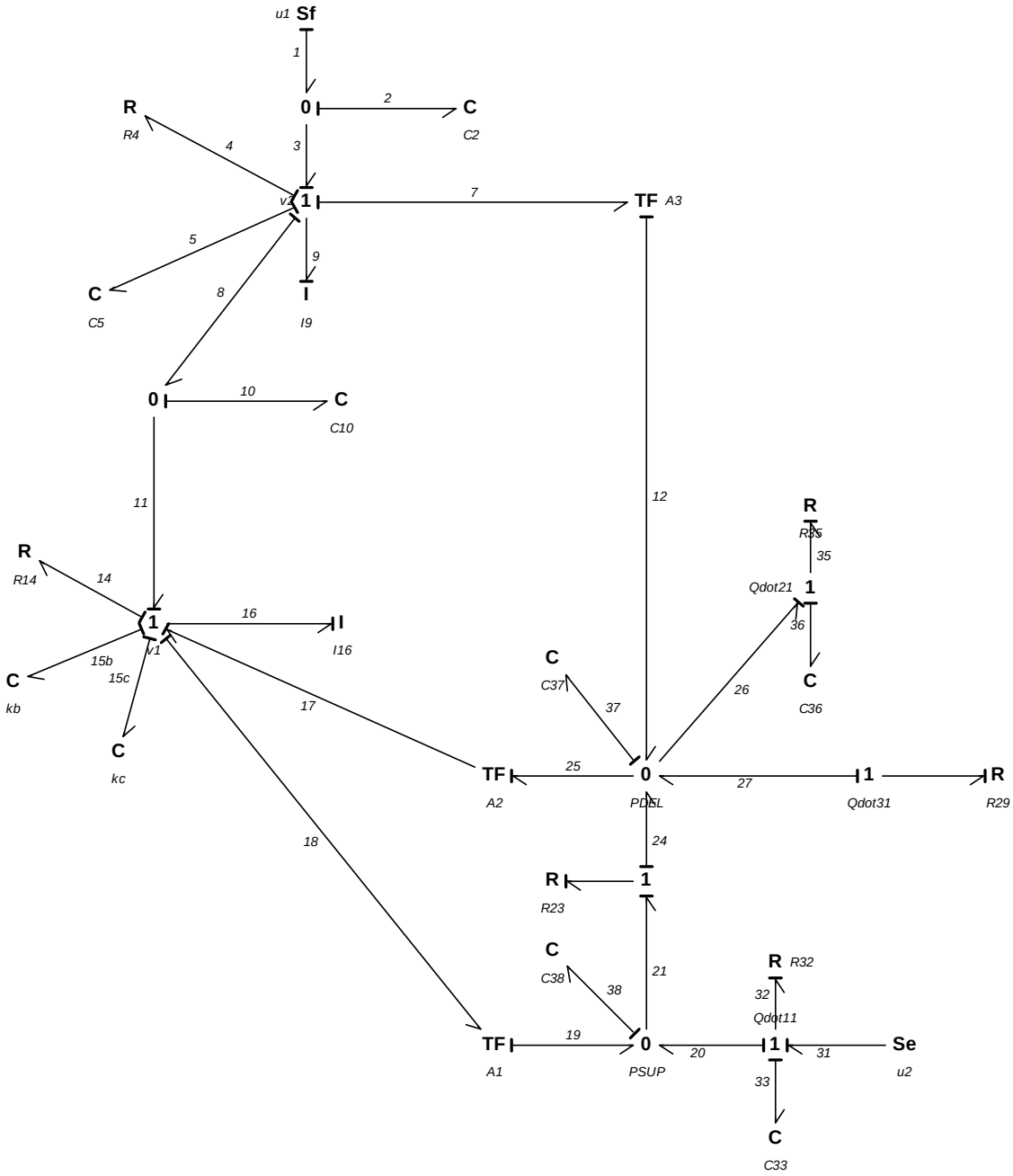

Figure 2.4: The Whole-System Bond Graph

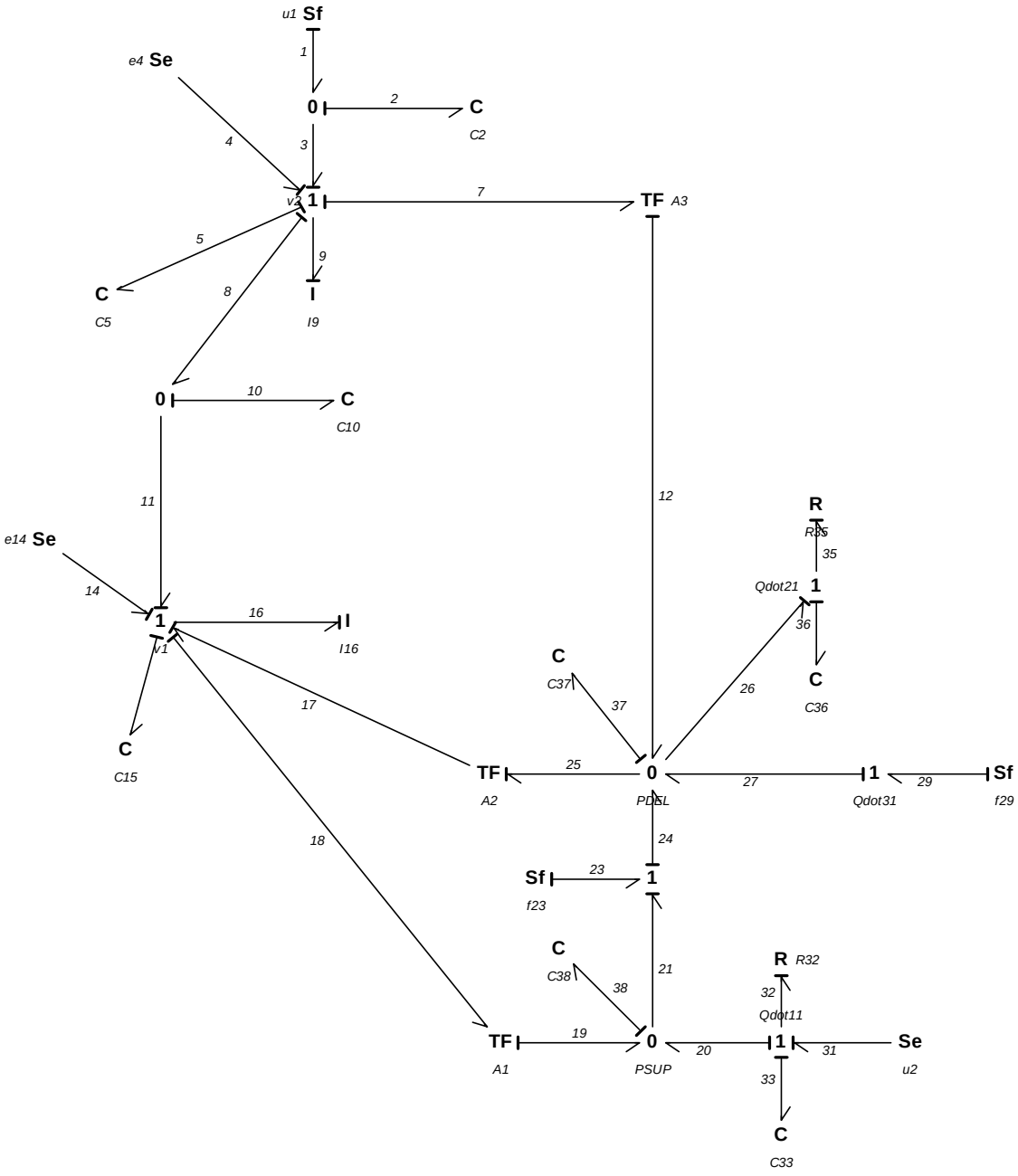

Figure 2.5: The completed bond graph

and aid in the generation of the state derivative equations.

2.4 Equation Formulation

The system is modeled as a state determined system. That is, it can be mathematically described by a set of ordinary differential equations in terms of the state variables and inputs. The augmented bond graph automatically determines the states. Each C element not in derivative causality generates a displacement state q_i and each I element not in derivative causality generates a momentum state p_i. For the valve being modeled this generates a vector of states shown in 2.2.

$$\mathbf{X} = \begin{pmatrix} q_{10} \\ q_{15} \\ q_2 \\ q_{33} \\ q_{36} \\ q_{37} \\ q_{38} \\ q_5 \\ p_{16} \\ p_9 \end{pmatrix} \tag{2.2}$$

and vector of inputs U,

$$\mathbf{U} = \begin{pmatrix} Sf_1 & = & u_1 \\ Sf_2 & = & u_2 \\ Se_3 & = & e_4(p_9) \\ Se_4 & = & e_{14}(p_{16}) \\ Sf_5 & = & f_{23}(q_{15}, u_2, q_{37}) \\ Sf_6 & = & f_{29}(q_{10}, q_{37}) \end{pmatrix} \tag{2.3}$$

A set of state derivatives can now be obtained by assuming the system is linear and using the 20-Sim software [1] to obtain A, B, C, and D matrices. With the linear matrices now obtained, 2.2 and 2.3 may be substituted into the compact form 2.4 to obtain the state derivatives for the linearized model.

$$\dot{\mathbf{X}} = A\mathbf{X} + B\mathbf{U} \tag{2.4}$$

Multiplying the state vector by the A matrix and the input vector by the B matrix gives the state derivatives in the explicit form.

$$\dot{\mathbf{X}} = f(X, U) \tag{2.5}$$

The equations generated by the multiplication are not however the final result for the nonlinear state derivatives. There are 3 nonlinear springs represented in the equations that must be manually corrected. The three springs are defined by bond graph efforts e_2, e_{10}, and e_{15}. The 10 state derivative equations obtained from 2.4 are inspected for terms containing the co-energy states; q_2, q_{10}, and q_{15} respectively. Those terms were then replaced with e_2, e_{10}, and e_{15} as appropriate. The result is as shown in

2.6.

$$\dot{\mathbf{X}} = \begin{pmatrix} \dot{q}_{10} &= & \frac{\mathrm{p_9}}{\mathrm{I_9}} - \frac{\mathrm{p_{16}}}{\mathrm{I_{16}}} \\ \dot{q}_{15} &= & \frac{\mathrm{p_{16}}}{\mathrm{I_{16}}} \\ \dot{q}_{2} &= & \mathrm{u_1} - \frac{\mathrm{p_9}}{\mathrm{I_9}} \\ \dot{q}_{33} &= & \left(\frac{-1}{R_{32}}\right)\left(\frac{\mathrm{q_{33}}}{\mathrm{C_{33}}} - \mathrm{u_2} + \frac{\mathrm{q_{38}}}{\mathrm{C_{38}}}\right) \\ \dot{q}_{36} &= & \left(\frac{-1}{R_{35}}\right)\left(\frac{\mathrm{q_{36}}}{\mathrm{C_{36}}} - \frac{\mathrm{q_{37}}}{\mathrm{C_{37}}}\right) \\ \dot{q}_{37} &= & \mathrm{f_{23}} + \mathrm{f_{29}} + \left(\frac{1}{R_{35}}\right)\left(\frac{\mathrm{q_{36}}}{\mathrm{C_{36}}} - \frac{\mathrm{q_{37}}}{\mathrm{C_{37}}}\right) - \frac{\mathrm{A2\,p_{16}}}{\mathrm{I_{16}}} + \frac{\mathrm{A3\,p_9}}{\mathrm{I_9}} \\ \dot{q}_{38} &= & \frac{\mathrm{A1\,p_{16}}}{\mathrm{I16}} - \left(\frac{1}{R_{32}}\right)\left(\frac{\mathrm{q_{33}}}{\mathrm{C_{33}}} - \mathrm{u_2} + \frac{\mathrm{q_{38}}}{\mathrm{C_{38}}}\right) - \mathrm{f_{23}} \\ \dot{q}_{5} &= & \frac{\mathrm{p_9}}{\mathrm{I_9}} \\ \dot{p}_{16} &= & \mathrm{e_{10}} + \mathrm{e_{14}} - \mathrm{e_{15}} + \frac{\mathrm{A2\,q_{37}}}{\mathrm{C_{37}}} - \frac{\mathrm{A1\,q_{38}}}{\mathrm{C_{38}}} \\ \dot{p}_{9} &= & \mathrm{e_2} + \mathrm{e_4} - \mathrm{e_{10}} - \frac{\mathrm{q_5}}{\mathrm{C_5}} - \frac{\mathrm{A3\,q_{37}}}{\mathrm{C_{37}}} \end{pmatrix} \tag{2.6}$$

2.5 Output

The model output is the effort at bond 36 which is a linear fluid compliance element representing the volume of the delivery line connected to the delivery port of the valve and any volume which may be connected to the opposite end.

$$y = e_{36} = \frac{q_{36}}{C_{36}} \tag{2.7}$$

CHAPTER III

SIMULATION DEVELOPMENT

Implementation of the model in a commercial numerical solver is relatively straight forward because all nonlinear elements are determined as functions of the state variables, all bonds are in integral causality, and there are no unassigned bonds. It has already been established that the model derived within this research is a state determined system. That means the response for all variables can be simulated with the already derived first-order state derivatives, state variable initial conditions, known input parameters, and algebraic equations relating the nonlinear variables to the state variables. The remaining unknowns required for simulation using a numerical integral time-step solver are determined in this chapter, a Matlab [15] script is written, a model is developed in Simulink.

3.1 Modes of Operation

The valve has three modes of operation and each is now evaluated in hydrostatic steady state in order to determine case dependencies for various terms in the set of state derivatives. The standard or nominal position is the balance or lap position depicted in 1.1. In this position all energy storage elements within the physical valve are active and all diameters contributing to bond graph transformer moduli are

also active. This means that the A_3 modulus is a surface area defined by the balance piston diameter D_4 less an area defined by the exhaust seal diameter D_2. The A_2 surface area is defined by a circular area having a diameter equal to the inlet seat D_1 less a circular area having a diameter equal to the exhaust seat D_2. The A_1 surface area is defined as a circular area having a diameter equal to the inlet seat D_1 less a circular area having a diameter equal to the barrel diameter of the poppet D_3.

$$A_3 = \frac{\pi}{4}(D_4^2 - D_2^2) \tag{3.1}$$

$$A_2 = \frac{\pi}{4}(D_1^2 - D_2^2) \tag{3.2}$$

$$A_1 = \frac{\pi}{4}(D_1^2 - D_3^2) \tag{3.3}$$

The release mode is identified by exhaust seal compression less than zero. The release mode is characterized by a clearance between the exhaust seat and the exhaust seal. The perpendicular surface area the delivery chamber is acting on is the entire area of the balance piston,

$$A_3 = \begin{cases} \frac{\pi}{4}(D_4^2 - D_2^2), & \text{if } q_{10} \geq 0 \\ \frac{\pi}{4}D_4^2, & \text{if } q_{10} < 0 \end{cases} \tag{3.4}$$

and the disk created by the inlet seat area minus the exhaust seat area is no longer present.

$$A_2 = \begin{cases} \frac{\pi}{4}(D_1^2 - D_2^2), & \text{if } q_{10} \geq 0 \\ 0, & \text{if } q_{10} < 0 \end{cases} \tag{3.5}$$

The behavior of the nonlinear spring effort e_10 is also dependent on the release mode

$$e_{10} = \begin{cases} e(q_{10})_{10}, & \text{if } q_{10} \geq 0 \\ 0, & \text{if } q_{10} < 0 \end{cases} \tag{3.6}$$

and also the exhaust flow.

$$f_{29} = \begin{cases} 0, & \text{if } q_{10} < 0 \\ f_{29}(q_{10}, q_{37}), & \text{if } q_{10} \geq 0 \end{cases} \tag{3.7}$$

The conditions for switching into release mode are presented here, but the formulation of the nonlinear equations for $e_1 0$ and $f_2 9$ is left for a later discussion in this thesis. The third mode of operation is the apply mode. The apply mode is defined by the exhaust orifice closed and the inlet orifice open. Like the case of the exhaust mode, some model parameters change in the apply mode. The defining state variable for the apply mode is inlet rubber compression q_{15}

$$A_1 = \begin{cases} \frac{\pi}{4}(D_1^2 - D_3^2), & \text{if } q_{15} \leq 0 \\ 0, & \text{if } q_{15} < 0 \end{cases} \tag{3.8}$$

Recalling that the compliance element C_{15} is comprised of a nonlinear rubber elastic element and linear helical spring element the e_{15} effort is now defined as dependent on q_{15},

$$e_{15} = \begin{cases} e_{15_c} - e_{15_b}, & \text{if } q_{15} \leq 0 \\ e_{15_c}, & \text{if } q_{15} > 0 \end{cases} \tag{3.9}$$

and also the inlet flow.

$$f_{23} = \begin{cases} f_{23}(q_{15}, u_2, q_{37}), & \text{if } q_{10} < 0 \\ 0, & \text{if } q_{10} \geq 0 \end{cases} \tag{3.10}$$

Again, the case dependency of the variables are only identified here and software formulation is left to a later discussion in this thesis.

3.2 Nonlinear Variables

There were 6 nonlinear terms in 2.6 that needed to be related to state variables in the vector 2.2. Each nonlinear term was manually investigated to find physical relationships with the states.

1. Sliding Friction of Balance Piston O-Ring e_4. The balance piston o-ring is modeled as sliding friction. Stick/slip behavior is not included in the friction model. The arctan function is substituted for the *signum* function which is not defined at 0 to aid in numerical simulation. The velocity term in the arctan argument is multiplied by a factor of 100 to make the transition from positive to negative sharper and closer in shape to the *signum* function. The multiplication factor can be decreased in simulation to improve simulation time for debugging or increased to improve accuracy.

$$e_4(p_9) = \frac{-2b_3}{\pi} \arctan(100 \times f_4) \tag{3.11}$$

Where b_3 is an estimate based on experimental measurement of the constant sliding friction of the o-ring along the inside wall of the valve body and f_4 is the flow variable of the resistive element. The negative sign is a result of the power half-arrow pointing away from the resistance 1-port element and toward the 1-junction in the final bond graph. Half-arrows should by convention point toward basic 1-port elements and away from source elements. Comparison of figures 2.4 and 2.5 show the direction of the power half-arrow changing direction when the R element is replaced with an effort source.

All nonlinear constitutive relations must be defined as functions of the state variables and inputs and f_4 from 3.11 is neither a state variable or input. It is however equal to f_9 which is a co-energy variable directly related to a state

variable by

$$f_9 = \frac{p_9}{I_9} \tag{3.12}$$

2. Sliding Friction of Poppet O-Ring e_{14}. The derivation of the nonlinear equation for the poppet body o-ring is similar to that of the balance piston o-ring above.

$$e_{14}(p_{16}) = \frac{-2b_2}{\pi} \arctan\left(100 \times f_{14}\right) \tag{3.13}$$

$$f_{14} = f_{16} = \frac{p_{16}}{I_{16}} \tag{3.14}$$

Again, the negative sign is a result of substituting an effort source for the original resistive force.

3. Inlet Flow Through an Orifice Restriction $f_{23}(q_{15}, u_2, q_{37})$. The generic form of fluid flow through an orifice used in this model 2.1 is adapted to provide the inlet flow specific to the inlet orifice and as a function of the state variables. The upstream (P_1) and downstream (P_2) pressures are related to fluid efforts

$$P_1 = e_{38} \tag{3.15}$$

$$P_2 = e_{37} \tag{3.16}$$

and the efforts are co-energy variables directly related to state variables.

$$e_{38} = \frac{q_{38}}{C_{38}} \approx u_2 \tag{3.17}$$

$$e_{37} = \frac{q_{37}}{C_{37}} \tag{3.18}$$

The orifice cross sectional area is also related to state variable q_{15} algebraically. The inlet orifice is open when the inlet seal is not in contact with the inlet seat. This occurs when the poppet body is displaced positively greater than the free

height of the rubber seal material. The inlet flow area is modeled simplistically as the side of a cylinder having a height equal to the clearance q_{15} between the rubber seal and inlet seat and a diameter equal to the inlet seat diameter D_1.

$$A(q_{15})_{inlet} = \pi D_1 q_{15} \tag{3.19}$$

Flow through the inlet orifice can now be explicitly written by substituting the above relationships into 2.1.

$$Q_{SUP} = f_{23} = A(q_{15})_{inlet}\sqrt{\frac{2}{\rho}|u_2 - e_{37}|}sgn(u_2 - e_{37}) \tag{3.20}$$

Typically flow through the inlet orifice will be from the supply chamber into the delivery chamber.

4. Exhaust Flow Through an Orifice Restriction $f_{29}(q_{10}, q_{37}, P_{exh})$. The generic form of fluid flow through an orifice used in this model 2.1 is adapted to provide the inet flow specifically based on the states. The upstream (P_1) and downstream (P_2) pressures are related to fluid efforts

$$P_1 = P_{exh} \tag{3.21}$$

$$P_2 = e_{37} \tag{3.22}$$

and the efforts are co-energy variables directly related to state variables.

$$P_{exh} = 0 \tag{3.23}$$

$$e_{37} = \frac{q_{37}}{C_{37}} \tag{3.24}$$

The orifice cross sectional area is also related to state variable q_{10} algebraically.

The exhaust orifice is open when the exhaust seal is not in contact with the exhaust seat which is based on the relative displacements of the balance piston and poppet body. Clearance occurs when exhaust rubber compression is less than zero. The exhaust flow area is modeled simplistically as the side of a cylinder having a height equal to the clearance $-q_{10}$ between the rubber seal and exhaust seat and a diameter equal to the exhaust seat diameter D_2.

$$A(q_{10})_{exhaust} = -\pi D_2 q_{10} \tag{3.25}$$

Flow through the exhaust orifice can now be explicitly written by substituting the above relationships into 2.1.

$$Q_{EXH} = f_{29} = A_{exhaust}(q_{10})\sqrt{\frac{2}{\rho}|P_{EXH} - e_{38}|}sgn(P_{EXH} - e_{38}) \tag{3.26}$$

Flow out of the delivery chamber in the valve will be a negative number as a result

5. Nonlinear Rubber Graduation Spring e_2. The force created by compression of the nonlinear rubber graduation spring is derived by experimentally measuring the force and compression q_2 of an actual sample using a tensile test machine and fitting a polynomial to the data using Matlab. Multiple orders of polynomials were fitted to the data using the Matlab $polyfit$ command. The best fit was obtained using a 4th order polynomial as seen in 3.1. The polynomial fitted to the data is

$$e_2 = 7.98 \times 10^{13} q_2^4 - 5.36 \times 10^{11} q_2^3 + 1.10 \times 10^9 q_2^2 - 4.34 \times 10^5 q_2 + 146.6. \tag{3.27}$$

The constant 146.6 is a problem for accurate modeling. The modeled spring will create a force equal to the constant when there is no compression. That is

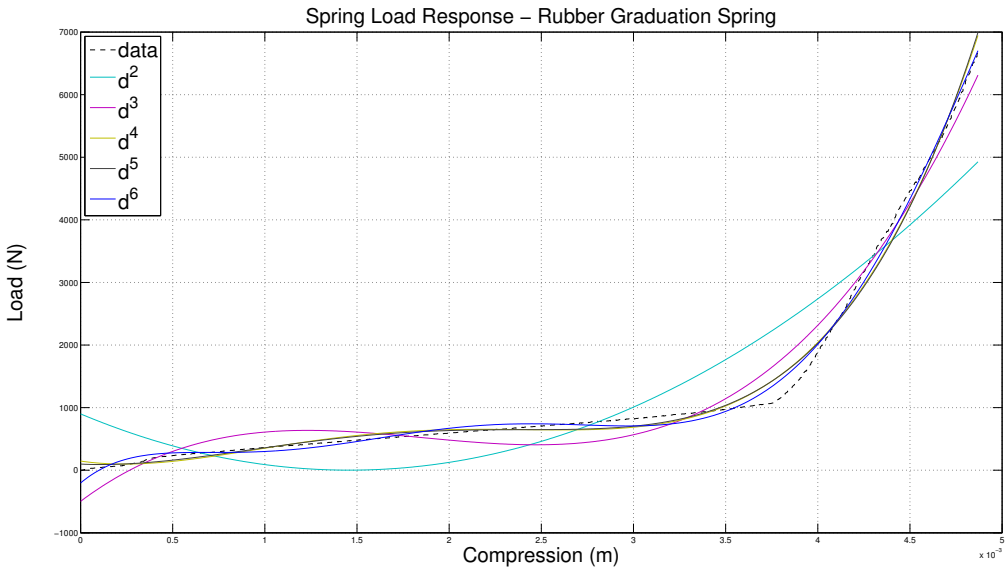

Figure 3.1: Rubber Graduation Spring Load vs. Compression Calibration Curve

not correct. A better solution is obtained by forcing the polynomial fit through the origin in order to obtain:

$$e_2 = 7.33 \times 10^{13} q_2^4 - 4.66 \times 10^{11} q_2^3 + 8.37 \times 10^8 q_2^2 - 7.27 \times 10^4 q_2. \qquad (3.28)$$

6. Nonlinear Spring Effect of Inlet Seal Rubber e_{15_b} and Exhaust Seal Rubber e_{10}. The rubber sealing material on top of the poppet creates a nonlinear spring effect when the elastic material is compressed q_{15} between the poppet body and the inlet seat. It also creates a similar spring-effect when the elastic material is compressed q_{10} between the exhaust seat and poppet body. Both springs are case dependent on whether the rubber seal material is in contact with the respective seat or not. An actual sample was measured using a tensile tester in a manner similar to the graduation spring to obtain a polynomial fit. The same polynomial is used in this thesis for the inlet seal and exhaust seal areas of the poppet.

$$e_{15_b} = 1.23 \times 10^9 q_{15}^2 - 3.84 \times 10^5 q_{15} + 10.9 \qquad (3.29)$$

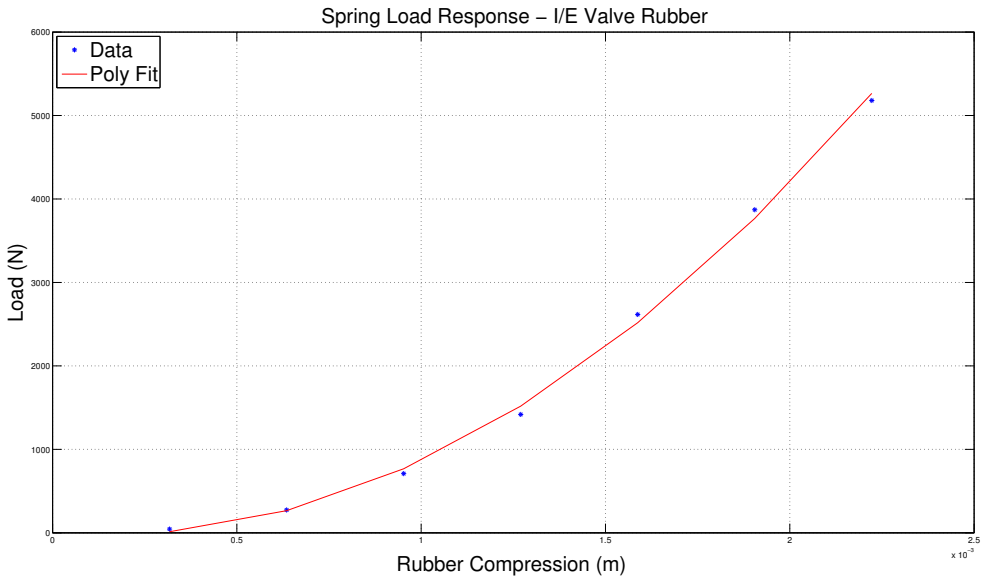

Figure 3.2: Rubber Seal Spring-Effect vs. Compression Calibration Curve

$$e_{10} = 1.23 \times 10^9 q_{10}^2 - 3.84 \times 10^5 q_{10} + 10.9 \tag{3.30}$$

3.3 Parameter Estimation

Regardless of whether the constitutive relation is linear or nonlinear, real parameters are required in order to obtain an accurate simulation. Some parameters are measured in U.S. customary units, but all calculations internal to the simulation are completed in metric units.

3.3.1 Linear Parameters

The remaining linear terms in 2.6 and Figure 2.5 need to be calculated. Regardless of which domain the parameter applies to, the linear relation is always maintained. Resistance is defined such that $e = R \times f$, compliance is defined such that $q = C \times e$, and inertia is defined such that $p = I \times f$. Details of linear parameter derivation used in this thesis are shown in Table 3.1.

Table 3.1: Linear Bond Graph Elements

TITLE	DEFINITION	UNITS
FLUID RESISTANCE	$R = 128\frac{\mu L}{D^4}$	$\frac{N-s}{m^5}$
MECHANICAL COMPLIANCE	$C = \frac{1}{k}$	$\frac{m}{N}$
FLUID COMPLIANCE	$C = \frac{V_0}{\rho_0 c_2}$	$\frac{m^5}{N}$
MECHANICAL TRANSLATION INERTIA	$I = m$	Kg
PISTON TRANSFORMER MODULUS: AREA	$A = \frac{\pi D^2}{4}$	m^2

3.3.2 Design Values and Research

Most of the geometry such as diameters and heights are obtained from engineering drawings of the valve sample being modeled. This is also true of linear spring rates for helical springs. Gas properties of compressed air are obtained from Wark [21]. In some cases such as gas reservoir volumes engineering judgment is exercised to provide realistic values. Masses used in the model are generally obtained via direct measurement with a scale. Rather than reproduce all of the obtained parameters and their sources here the reader is directed to the Matlab code in appendix B which is annotated with the sources of all parameters.

3.4 Initial Conditions

The valve is in steady state and in the full release mode to begin the simulation. All masses are zero velocity, spring compressions can be calculated from known geometry of the valve, and initial fluid displacements can be similarly calculated. Those calculations are used as first estimates and a steady state simulation is run with constant zero velocity for the u_1 input and a constant 120 psi for the reservoir pressure input u_2. Excessive oscillations for some of the states at the start of the steady state simulation indicate that some of the assumptions used in the calculations were not completely accurate. Simulink plots are used to find updated steady state values. Details regarding each of the steady states are described in the subsections

within this section. Atmospheric conditions for all simulations and experiments are 20°C and 1atm unless otherwise noted.

3.4.1 q_{10} - Spring Compression, Exhaust Seal

In the full release operating mode of the valve the exhaust has a clearance with the exhaust seal rubber. A first estimate of initial compression of the exhaust seal rubber material is obtained by calculating the position of the exhaust seat relative to the zero reference and assuming the top of the rubber material is at the zero reference. The steady state simulation is used to determine the final value for simulation.

3.4.2 q_{15} - Displacement, Poppet Body

The displacement of the poppet body q_{15} is used to calculate the compression of two springs; the spring effect of the rubber sealing material of the inlet valve, and the linear helical body return spring. The zero displacement reference of the poppet is carefully chosen as the plane created by the inlet seat. This selection means that the poppet displacement is also equal to the compression of the rubber. The spring effect due to the rubber of the inlet seal is in compression (negative value) with the valve in the full release position. A first estimate for the initial condition is obtained by balancing the forces on both sides of the poppet and solving for compression (q_{15}) using the experimentally measured non-linear spring equation.

3.4.3 q_2 - Spring Compression, Graduation Spring

The initial compression for the rubber graduation spring is found be setting $\dot{p}_9 = \mathrm{e2} + \mathrm{e4} - \mathrm{e10} - \frac{\mathrm{q5}}{\mathrm{C5}_c} - \frac{\mathrm{A3}_r\,\mathrm{q37}}{\mathrm{C37}_c} = 0$, substituting the known equation for e_2, and solving for q_2.

3.4.4 q_{33} - Gas Standard Volume, Supply Line

Fluid compliance is based on the equation $C_{33} = \frac{V_0}{\rho_0 c^2}$ where V_0 is the volume of the container or supply line which is a known value based on the higher level system model, ρ_0 is the density of the gas at atmospheric conditions, and c is the speed of sound in the gas at atmospheric conditions. The initial condition V_{33} is determined by solving the linear relation $V_{33} = \frac{P_{33}}{C_{33}}$ where P_{33} is the defined initial pressure setting of the u_2 input and C_{33} is the previously calculated fluid compliance value.

3.4.5 q_{36} - Gas Standard Volume, Delivery Line

Fluid compliance specific to the delivery line is again calculated similar to that of the supply line; $C_{36} = \frac{V36_0}{\rho_0 c^2}$. Where $V36_0$ is the volume of the delivery line, ρ_0 is the density of the gas at atmospheric conditions, and c is the speed of sound in the gas at atmospheric conditions.

3.4.6 q_{37} - Gas Standard Volume, Delivery Chamber

The calculation of the initial gas standard displacement volume of the valve delivery chamber is similar to that of the delivery line, but with a much smaller container volume.

3.4.7 q_{38} Gas Standard Volume, Supply Chamber

The calculation of the initial gas standard displacement volume of the valve supply chamber is similar to that of the supply line, but with a much smaller container volume.

3.4.8 q_5 - Spring Compression, Piston Return

The piston return spring is a linear helical spring with one non moving end seated on a surface within the valve body and the second end seated on the underside of the balance piston. The initial compression is found by subtracting the initial spring working height from the spring free height. Both are known values based on geometry of the valve.

3.4.9 p_9 - Mass Momentum, I/E Valve

All masses are at zero translation and rotational velocity to begin the simulation. Therefore the initial momentum is also zero.

3.4.10 p_{16} - Mass Momentum, Primary Piston

All masses are at zero translation and rotational velocity to begin the simulation. Therefore the initial momentum is also zero.

3.5 Software Code

Simulink is well suited for simulating the model based on the 10 nonlinear state derivatives. The system as modeled in Simulink is shown in Figure 3.3. All of the logic and equations needed to write the user defined function code in Matlab are already established in the earlier discussions in this thesis. Consistent with the bond graph, equation formulation, and Simulink model the user defined Matlab function provides an output of 10 state derivatives $\dot{X}$ and the system output e_{36} and requires as inputs a vector of two independent variables as well as feedback of the 10 state variables. The integration is performed using the Simulink ode45 numerical solver with variable step size.

The 3 bond graph transformer moduli case dependencies were written in the Matlab function however it was noticed that the case dependency tended to cause an unnatural and unrealistic oscillation in Simulation during valve release. In the real physical system the valve does not instantaneously switch between modes of operation with respect to the equivalent areas as they are described in section 3.1. The modes of operation were evaluated hydro-statically which is not a real condition in the valve. Pressure will vary with time and across the surface area of the piston; especially during transitions from one operation mode to another. A more accurate model would add considerable complexity without adding greater understanding of the operation of the valve. The balance piston surface area $A3$ is instead always modeled as though it was in the nominal lap position.

The Simulink model includes outputs to the workspace for both the input pressure and integral of the plunger input velocity. Plunger displacement is typically used to study valve response whereas velocity has little practical meaning.

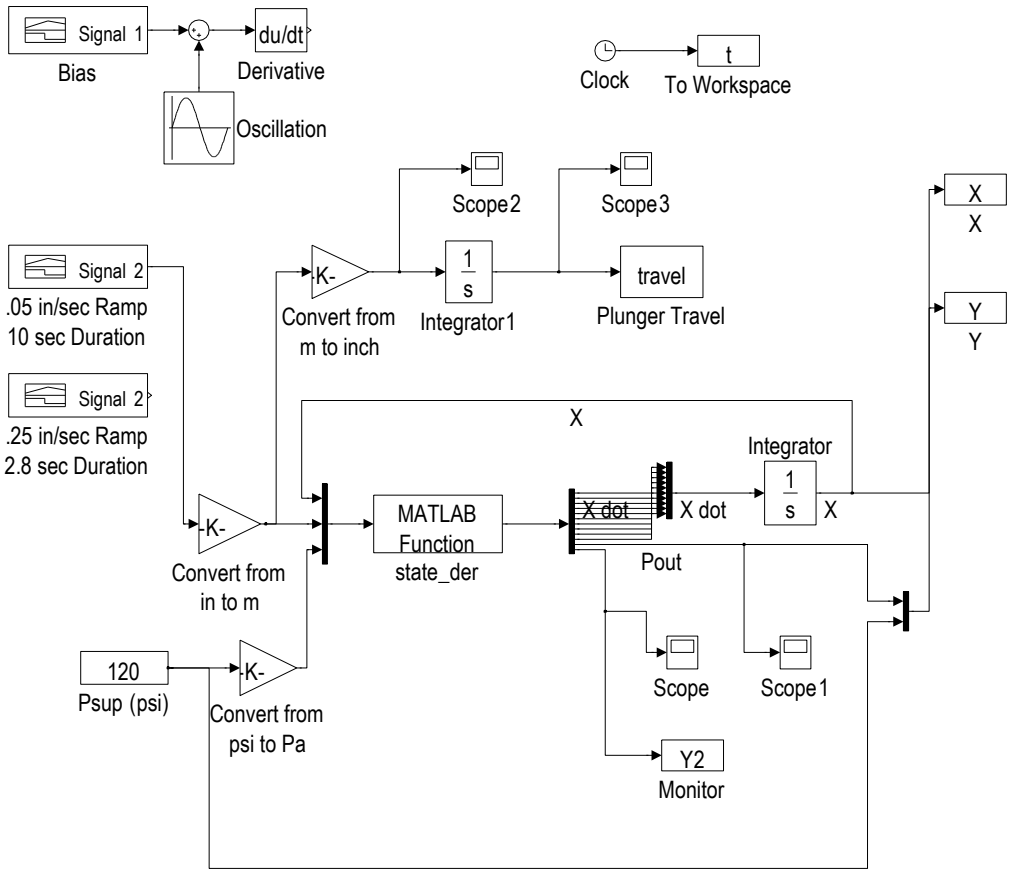

Figure 3.3: Simulink Model for a System of 10 Nonlinear State Derivatives

CHAPTER IV

RESULTS AND DISCUSSION

This chapter uses the model developed in chapters II and III to execute simulations, and compare and tune the model to an actual valve. The tuned model is then used to evaluate the dynamic performance of the valve.

4.1 Tuning and Optimization

The model was first simulated in a semi-static condition to evaluate how closely it matched the known physical sample. The travel velocity or u_1 flow source was set to apply at a rate of .08 in/sec for a duration of 5 seconds then released at the same rate for the same duration to return to the initial position. A short dwell was added at the beginning and end of the input signal in order to verify the model was in steady state to begin the simulation. The result is shown in figure 4.1.

The shape of the profile was not quite as what was expected from the physical valve. The semi-static profile is primarily driven by the characteristic equation for the nonlinear rubber graduation spring, so 3.28 was inspected to find the source of the inconsistency. It can be seen in Figure 3.1 that although the 4th order polynomial fits the curve closely, the modeled spring force actually decreases with increasing compression for smaller compressions with a local minimum at .0021m compression.

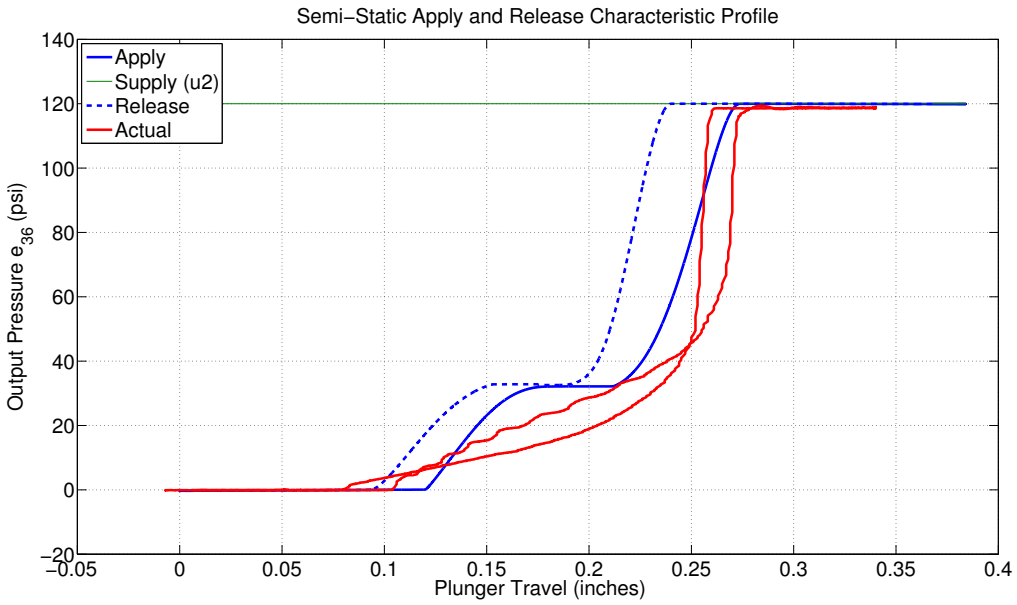

Figure 4.1: Semi-Static Pressure Response of Valve Model Without Tuning

The modeled spring behavior did not match what was expected and it affected the overall model. A new spring model was developed to correct the behavior of load vs. compression curve e_2. The new spring model was based on two linear models with an inflection point at $q_2 = .003759m$ and $e_2 = 1076N$.

The general shape of the performance profile of the valve in figure 4.2 was visually more accurate when using a compound linear equation set for the nonlinear spring rate than by using a single polynomial fit of Figure 4.1. Increasing plunger travel produced increasing pressure for all points. This is the behavior that is expected from the proportional pressure modulating valve. A semi static experiment with a physical sample was superposed on the plot and it was observed that the shape did not match. Further tuning was required.

The model derived in this thesis, and physical system described in section 2.2 do not match the physical valve used in the experiment. The valve used in the experiment is coupled to a second pneumatic circuit through a relay piston and the coupling may have an effect on the performance of the first circuit which is modeled

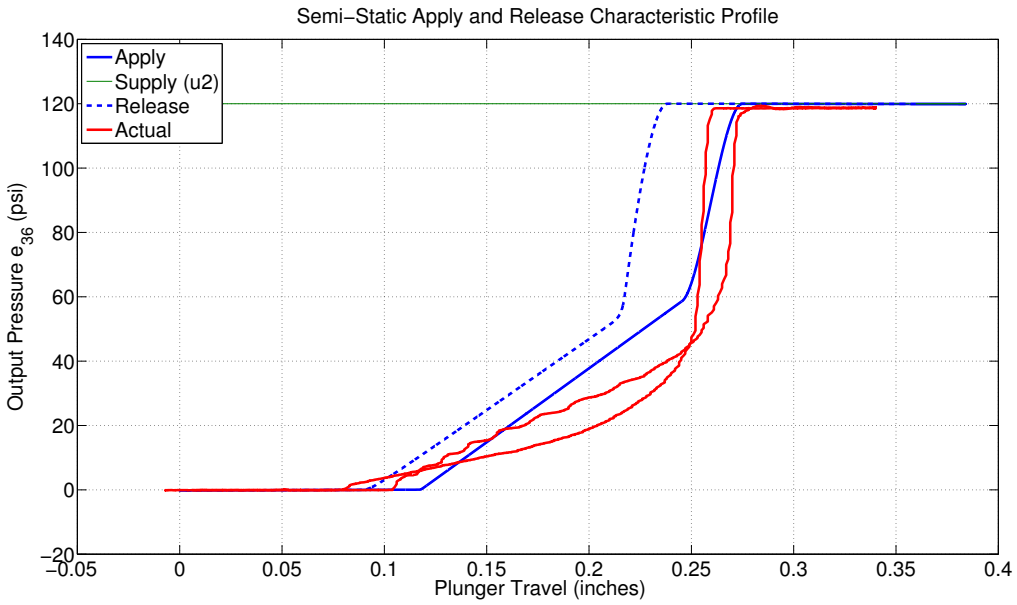

Figure 4.2: Semi-Static Pressure Response with Compound Linear Model for e_2

in this thesis. Some components in the physical valve are not included in the model. The model geometry was modified to tune the behavior to the physical sample by increasing the diameter of the balance piston to 3.0 inches.

Figure 4.3 shows the optimized response of the model to a semi-static apply and release cycle. It is a close match with the physical sample and was accepted as the best fit model although there are still noticeable differences between the model and the physical experiment. The release curve did not cross the apply curve, and travel hysteresis during the transition from apply to release was greater in the model than in the physical experiment. Both of these discrepancies are explained by the assumptions and simplifications identified in 2.1. In a real valve static friction holds the balance piston in place as the direction of motion is changed from apply to release. Once the critical force is overcome the balance piston moves up and the exhaust orifice is opened a relatively large amount. Gas flows out of the exhaust and briefly allows the pressure to drop below what is expected by the releasing plunger travel before the valve returns to a smooth modulating type of behavior. The model however does not

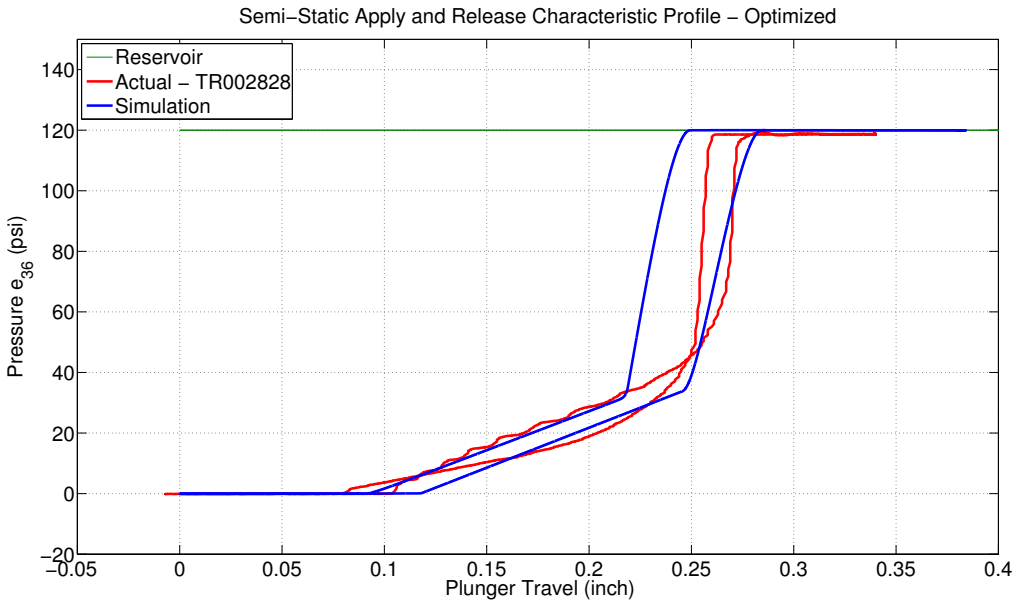

Figure 4.3: Semi-Static Pressure Response with Optimized Compound Linear Model for e_2

include stick/slip friction. The exhaust orifice opens gradually and allows gas flow to be smoothly exhausted.

The increased travel hysteresis is explained by the simplification of the variable inlet and exhaust restrictions as turbulent flow through orifices. The constitutive relation 3.26 includes multiplication by the cross section area. The model inherently assumes the seats make perfect seals with the rubber, and exhaust flow only occurs once the poppet sealing material is not in contact with the exhaust. That is not the case in a real valve. In a real valve compressed air will begin to flow while the exhaust seat is still mostly in contact with the sealing material. A considerable amount of design effort is used in the design of the seat geometry and tolerances, and material properties of the sealing material to balance the conflicting objectives of good seal and durability. In the model the release cycle only begins once the force on top of the balance piston has decreased enough to change the relationship between the exhaust seat and exhaust seal from compression to clearance.

4.2 Dynamic Analysis

This is a dynamic model and intended to study the dynamic behavior of the valve in a higher level system. Figure 4.4 shows the result of a dynamic apply and release. The ramp rate is changed from .08in/sec in the semi-static simulation to 2 in/sec in the dynamic simulation. When excited with this faster input rate the pressure response lags behind the input travel both in the apply and release directions which is what is expected.

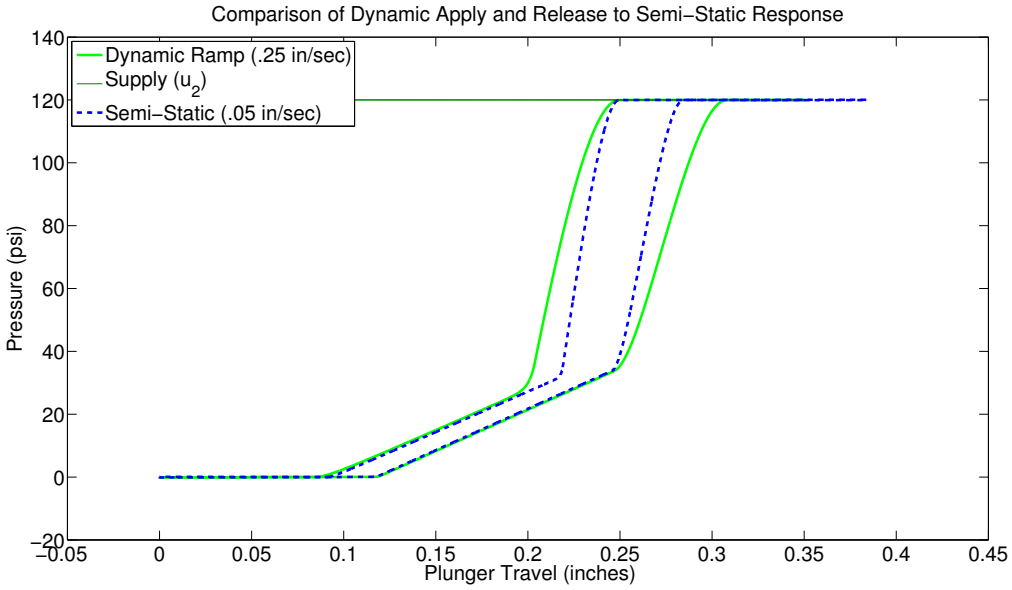

Figure 4.4: Comparison of Dynamic Pressure Response to Static Response

The input ramp is replaced with a low frequency sinusoidal input to further investigate the transient behavior of the valve. The valve type modeled in this thesis is considered appropriate for operation in low frequency and is not typically used in high frequency applications. The type of valve design modeled in this thesis is typically used in low frequency applications under 1 hz. The following series of simulations demonstrate the effect of input frequency on the response of the valve. A sine wave of 4 rad/s and amplitude of .07 inches was modeled as a nominal input. The input was changed from a velocity or travel rate to input plunger position and the position input

was differentiated to create the input flow source. The sinusoidal position input was summed with a position ramp of 0.2 inch over 1 second so that the input oscillation stayed within a position band of 0.1 - 0.3 inches to avoid the semi-static limits of full apply and zero apply pressures observed in figure 4.3. The actual minimum and maximum of the oscillating input used in the simulation were 0.13 inches and 0.27 inches of plunger travel.

Figure 4.5 shows the response of the modeled valve to the oscillating input described above. The maximum pressure output of the oscillating response is $110.6psi$ and the peak output lags behind the peak input by $0.14sec$ as seen in figure 4.6. The steady state pressure output of the valve at 0.27 inches of plunger travel is actually less than the peak dynamic response in figure 4.5. A possible explanation for this would be a delay or lag in the time for the piston to move from an inlet open / exhaust closed position in the dynamic simulation. Net fluid flow continues to be into the delivery or output side of the valve even when plunger position and output pressure would indicate zero flow or net exhaust fluid flow.

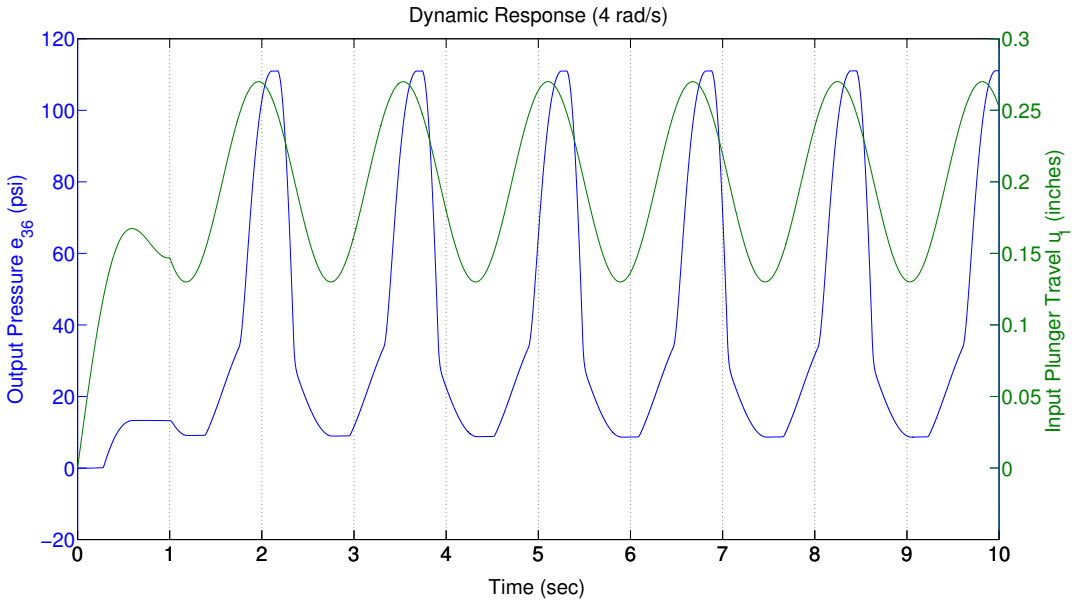

Figure 4.5: Response of Valve to Sinusoidal Input $\omega = 4rad/s$

An objective estimate of system dynamic performance at this frequency was

obtained by inspecting the sinusoidal response closely in Figure 4.6 to determine the system gain:

$$Gain = \frac{Output}{Input} = \frac{111psi}{.275in} = 403\frac{psi}{in} \tag{4.1}$$

The sinusoidal position input is changed to a higher frequency of 8 rad/sec while

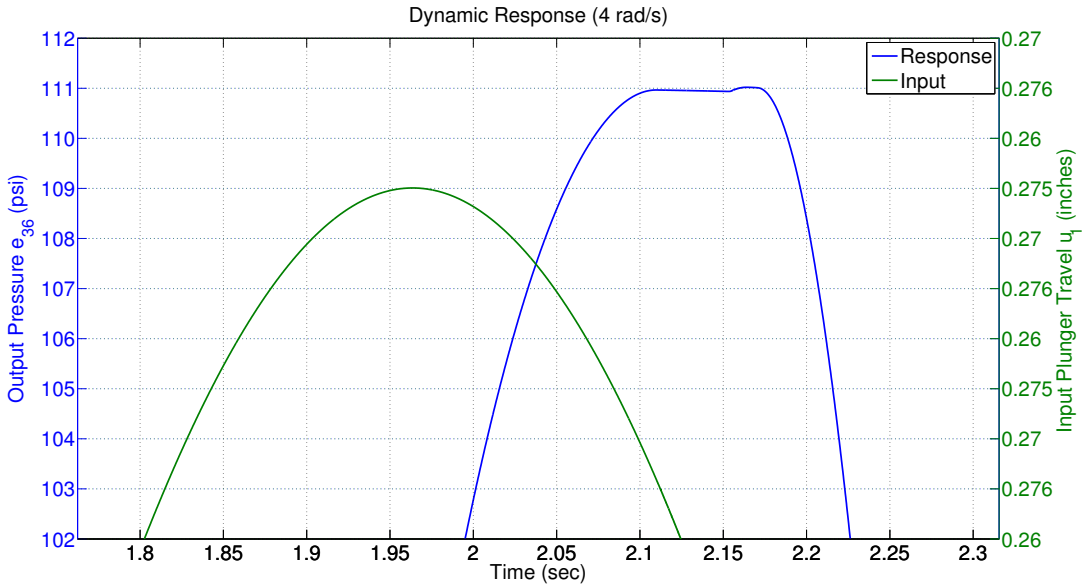

Figure 4.6: Response of Valve to Sinusoidal Input - Peak Output and Time Lag $\omega = 4rad/s$

maintaining the same input signal amplitude in the next simulation and it is clear why the valve is not suitable for higher frequency applications as the amplitude of the valve response drops to 93.1 psi at this still relatively low frequency input signal.

$$Gain = \frac{Output}{Input} = \frac{93.1psi}{.275in} = 338\frac{psi}{in} \tag{4.2}$$

Finally, the input frequency is changed to 20 rad/sec while maintaining the same input signal amplitude and the system response is observed as before:

$$Gain = \frac{Output}{Input} = \frac{68psi}{.275in} = 247\frac{psi}{in} \tag{4.3}$$

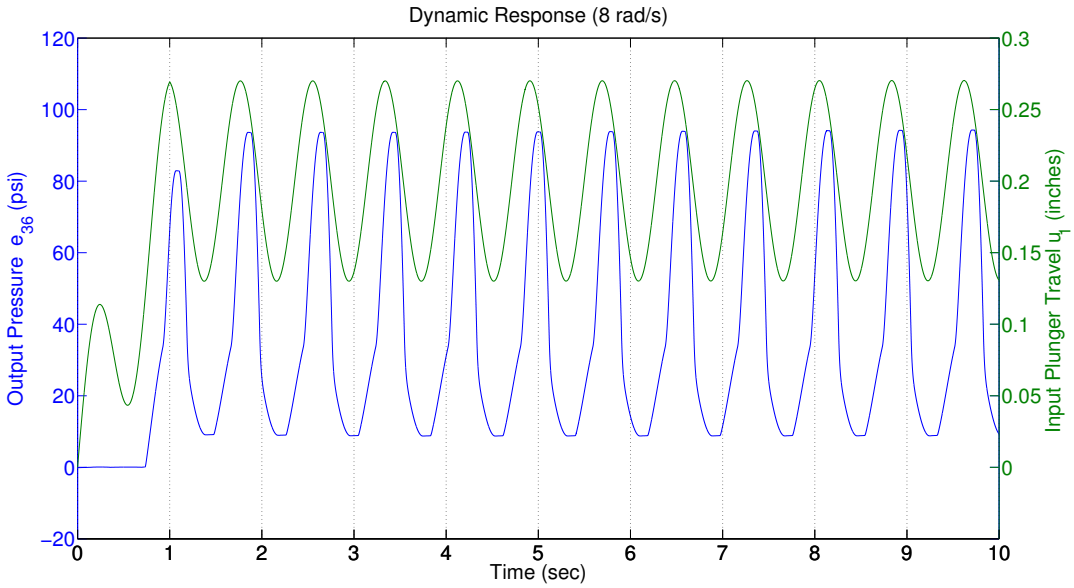

Figure 4.7: Valve Response to Higher Frequency Sinusoidal Input $\omega = 8rad/s$

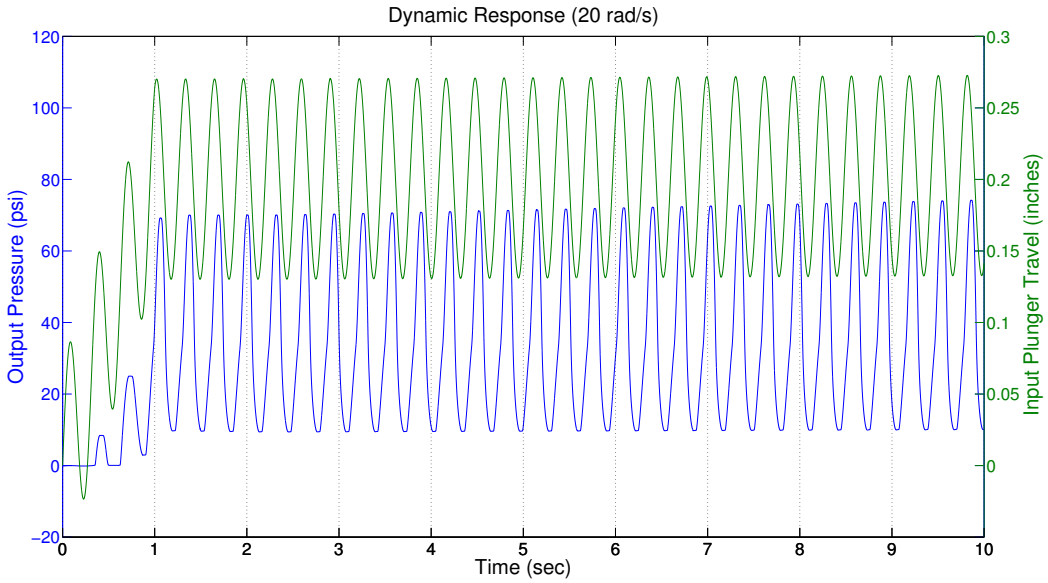

Figure 4.8: Valve Response to Higher Frequency Sinusoidal Input $\omega = 20 rad/s$

CHAPTER V

CONCLUSIONS AND FUTURE WORK

5.1 Conclusions

The primary research objectives of this thesis were achieved. A model was developed that is adaptable, upgradeable based on future developments, and can be coupled with other components in a higher-level system. The bond graph method was used to study a system that was comprised of two different energy domains; mechanical translation and pneumatic fluid power. Nonlinear behaviors in both the mechanical and pneumatic halves of the model were studied and acceptable relationships were derived. The mathematical model was adapted for computer simulation. Finally, the model was demonstrated to behave similarly to a physical valve and a dynamic simulation was used to examine the behavior of the valve.

The model is adaptable. Subsystems for the piston, poppet, and pneumatic circuit were developed. The subsystems based on basic physical elements such as damping, compliance, and inertia could be applied to any number of valves.

The model is upgradeable based on future research and developments. The state derivative equations developed in this model included nonlinear elements left as variables in the simulation. The nonlinear equations developed for those variables in this thesis may easily be replaced if they are not suitable for future applications.

The model can be coupled with other components in a higher-level system. The input plunger velocity variable in this thesis designed as an independent source can be replaced with an output from an upstream device. The constant input pressure can be replaced with a model for an actual reservoir on pneumatic line. The output volume can be easily be replaced with a downstream device model such as another valve or actuator.

The developed model was used to demonstrate through simulation that the physical valve function is limited at higher frequency inputs. Frequency analysis of the valve response would not be possible with static models of the valve such as those that previously existed as this utility is only available with dynamic models. Existing black-box models of the valve would be able to demonstrate the frequency limitations of the valve, but only after a physical sample was built. Those same black-box models would not be of much value with respect to design changes to improve the responsiveness of the device. The engineer would have only an unsatisfactory simulation result, and an abstract second order differential equation with which to fix the problem. The simulation in this thesis however allows the user to modify any number of parameters and observe relatively quickly whether there is an expected improvement in performance.

5.2 Future Work

The model was demonstrated to be substantially accurate through a comparison of simulation to an actual valve and the model would be appropriate for some product design work. However, the model as described in this thesis would like not be suitable for some uses such as control design. The small inaccuracies between the model and the actual valve with regards to hysteresis and internal fluid flow would need to be corrected.

Areas for improvement of the model were identified by inspecting the simulations in Chapter IV. In particular, the analyses of the nonlinearities were kept at the simplest level possible and future work could be completed to improve the accuracy of the model. The simple sliding friction model can be improved to include stick/slip characteristics. The lack of stick/slip in the friction model was identified as a likely contributor to a noticeable discrepancy between the optimized simulation and actual valve. Various friction models which lend themselves to numeric simulation and include stick slip are available in the published literature.

Another opportunity to upgrade the model is the fluid flow equations for the inlet and exhaust restrictions. The analytic model used in this research was used for simplification, but a more accurate model would be based on experimentation and would present the flow model as a surface dependent on both upstream/downstream pressure differential and sealing force.

The model created in this thesis is intended to be used as part of a higher-level system model. Fluid momentum was not included in the model in this thesis, but it may be a necessary element in a higher-level system model. The bond graph method may also be used to develop system models of the pneumatic lines used to connect devices in a compressed air system. The next step in developing a higher level system model should include development of the pneumatic line models with fluid momentum included. Finally, the model should be compared to an actual valve in dynamic cycling with parameter optimization.

BIBLIOGRAPHY

[1] 20-Sim, *version 4.4.2*, Controllab Products B.V., 2014.

[2] P. Beater, *Pneumatic drives: System design, modeling and control*, Springer, 2007.

[3] T.K. Bera, A.K. Samantaray, and R. Karmakar, *Bond graph modeling of planar prismatic joints.*, Mechanism & Machine Theory **49** (2012), 2 – 20.

[4] Wolfgang Borutzky, *Bond graph methodology: Development and analysis of multi-disciplinary dynamic system models*, 2010.

[5] Shuvra Das, *Mechatronic modeling and simulation using bond graphs*, Taylor & Francis Group, LLC, 2009.

[6] Donal L. Margolis Dean C. Karnopp and Ronald C. Rosenberg, *System dynamics: Modeling and simulation of mechatronic systems*, John Wiley & Sons, Inc., 2006.

[7] J. Feldmann and B. Kiel, *Brake signal transmitter with integrated addition redundancy*, March 12 2002, US Patent 6,354,671.

[8] H.J. Goebels and C.M. Knaack, *Control module for single 3/2 solenoid controlled relay valve*, August 18 2009, US Patent 7,577,509.

[9] Majed M. Hamdan, *Moddified pid control of pneumatic valves with hysteresis*, Master's thesis, CSU.

[10] Duane R. Johnson, *Basic e-6 and e-7 theoretical performance curve tolerance band calculations*, Bendix Commercial Vehicle Sytsems LLC, July 1986.

[11] Bendix Commercial Vehicle Systems LLC, *Service data: E-6 & e-10 dual brake valves sd-03-817*, 2007.

[12] D. Margolis, *Bond graphs, modeling, and simulation in industry: some examples where costly mistakes could have been avoided*, Systems, Man and Cybernetics, 2002 IEEE International Conference on, vol. 3, Oct 2002, pp. 5 pp. vol.3–.

[13] ———, *Why physical system modeling is important to industry: Bond graph models that could have prevented some costly mistakes*, Control 2010, UKACC International Conference on, Sept 2010, pp. 1–6.

[14] Donald L. Margolis, *Bond graph fluid line models for inclusion with dynamic systems simulations*, Journal of the Franklin Institute **308** (1979), no. 3, 255 – 268.

[15] MATLAB, *version 8.1.0.604 (r2013a)*, The MathWorks Inc., Natick, Massachusetts, 2013.

[16] H. Olsson, K.J. strm, C. Canudas de Wit, M. Gfvert, and P. Lischinsky, *Friction models and friction compensation*, European Journal of Control **4** (1998), no. 3, 176 – 195.

[17] T.L. Peabody, *Using amesim modeling software to study the effect of line sizing and valve placement on the operation of a 53ft slide axle trailer air brake system*, Bendix Commercial Vehicle Sytsems LLC, December 2008.

[18] G. Heydinger M. Salaani S. Chandrasekharan, D. Guenther, *Development of a roll stability control model for a tractor trailer vehicle*, SAE Int. J. Passeng. Cars Mech. Syst. 2(1):670-679 (2009).

[19] S. Narayanan S. Sridhar and B. Kumaravel, *Dynamic simulation of a brake valve in air brake system*, SAE Technical Paper 2009-28-0030 (2009).

[20] Yasuo SAKURAI, Yoshitaka HANEISHI, Kazuhiro TANAKA, Takeshi NAKADA, and Takehisa KOHDA, *Simulation of dynamic characteristics of air gripper by a new bond-graph method.*, **2008** (2008), no. 7-3, 747 – 752.

[21] Kenneth Wark, *Tables and figures to accompany thermodynamics*, McGraw-Hill Inc., 1988.

[22] Zhu Yong and Eric J. Barth, *Passivity-based impact and force control of a pneumatic actuator.*, Journal of Dynamic Systems. Measurement and Control **130** (2008), no. 2, 1.

APPENDIX A

CONSTITUTIVE EQUATIONS

Table 1.1: Basic 1-Port and 2-Port Elements of the Bond Graph

BRIEF DESCRIPTION	BOND	CAUSAL RELATION
SOURCE - MECHANICAL VELOCITY, PLUNGER	1	$f_1(t)$
COMPLIANCE - SPRING, RUBBER GRADUATION	2	$e_2 = \Phi_c^{-1}(q_2)$
RESISTANCE - COULOMB FRICTION, O-RING	4	$e_4 = \Phi_R(p_9)$
COMPLIANCE - SPRING, HELICAL PISTON RETURN	5	$F_5 = k_e X(q_5)$
INERTIA - MASS, BALANCE PISTON	9	$f_9 = \frac{p_9}{m_p}$
COMPLIANCE - SPRING, RUBBER EXHAUST	10	$e_{10} = \Phi_c^{-1}(q_{10})$
RESISTANCE - COULOMB FRICTION, O-RING	14	$e_{14} = \Phi_R(p_{16})$
COMPLIANCE - SPRING, HELICAL POPPET RETURN	15_c	$F_{15_c} = k_e X(q_{15})$
COMPLIANCE - SPRING, RUBBER INLET	15_b	$e15_b = \Phi_c^{-1}(q_{15})$
COMPLIANCE - SPRING, RUBBER EXHAUST	10	$e_{10} = \Phi_c^{-1}(q_{10})$
INERTIA - MASS, POPPET	16	$f_{16} = \frac{p_{16}}{m_{LE}}$
RESISTANCE - FLUID FLOW, INLET	23	$f_{23} = \Phi_R^{-1}(q_{15}, u_2, q_{37})$
RESISTANCE - FLUID FLOW, EXHAUST	29	$f_{29} = \Phi_R^{-1}(q_{10}, q_{37})$
SOURCE - FLUID PRESSURE, SUPPLY	31	$e_{31}(t)$
RESISTANCE - FLUID, SUPPLY LINE	32	$P = R_{32} Q_{SUP}$
COMPLIANCE - FLUID, SUPPLY LINE	33	$P_{33} = \frac{V(q_{33})}{C_{33}}$
RESISTANCE - FLUID, DELIVERY LINE	35	$P = R_{35} Q_{OUT}$
COMPLIANCE - FLUID, DELIVERY LINE	36	$P_{36} = \frac{V(q_{36})}{C_{36}}$
COMPLIANCE - FLUID, DELIVERY CHAMBER	37	$P_{37} = \frac{V(q_{37})}{C_{37}}$
COMPLIANCE - FLUID, SUPPLY CHAMBER	38	$P_{38} = \frac{V(q_{38})}{C_{38}}$

APPENDIX B

MATLAB PROGRAMS AND SIMULATION MODELS

```
function [out] = A7_2_state_der(X, U)
% TITLE: Non Linear State Derivatives for Modeling of a Pneumatic,
% Continuously Variable, Pressure Modulating Valve
% Created By: Chris Brubaker | Student ID 2581277
% Date Created: April 15, 2015
% Revised: April 15, 2015
%
% DETAILED DESCRIPTION: This Matlab function may be used as a user defined
% Simulink function block to calculate the state of the foot brake valve.
% The non-linear state space equations were developed separately using the
% bond graph technique and the linearization tool in 20-Sim.  Features of
% the A7 model include adjustments to the state derivative equations to
% remove the effects of fluid inertia from the model.  The number of states
% is reduced from 12 in the A6_2 model to 10 in in the A7_1 model.
%
%INPUTS:
% - X: The state values from the previous iteration (10 X 1)
% - U: The actual inputs u1 (plunger travel) and u2 (reservoir pressure)
%
% OUTPUTS:
% - xdot: A 10 X 1 array of the state derivatives
% - Y: A 2 X 1 array
%      1.) Pressure in the delivery line (psi)
%      2.) Supply Pressure (psi)
%
% CUSTOM LIBRARY FUNCTIONS REQUIRED:
% - None
```

```
%
% REFERENCE FILES:
% - A7_1_bond graph.emx
% - A7_1_initialize.m
% - A6_2_linearization.m
% - A6_2_xdot.m
%
% REVISIONS:
%04/15
% - Copy script from A7_1_state_der.m model; create A7_2 model.
% - Change sign convention for all terms affected by TF:A2 bonds.
% - Incorporate power arrow direction change included in the A7_2 model.
% - Change state-derivative and state variable vector sizes from 12 to 10.
% - Remove p30_0 and p34_0 from the initial condition vector.
% - General script clean-up to remove or "comment out" unused parameters
%   and equations.
%=========================================================================
%04/15
% - Archive A7_1 Model.
%04/09
% - Change the f29 exhaust flow calculation to correctly change sign based
%   on relative upstream and downstream pressures.
% - Remove case dependency for balance piston effective area A3.
% - Tune the model by changing D4 to 3.0 inch from 2.375 inch.
% - Tune the static response by replacing graduation spring polynomial with
%   compound linear spring-force model.
%04/01
% - Change the sign convention in the calculation of Ae and subsequent
%   calculation of f29 to eliminate confusion caused by use of "negative"
%   area.
% - Removed 1000X factors from A11 & A22 calcs. (only used with fluid
%   inertia).
% - Changed e2 force polynomial to be constrained to go through the origin.
%03/13
% - Added operation mode case dependency for A3.
% - A2 Changed to a negative value to account for direction of power arrow
%   in bond graph.
% - Travel limits for q5 supressed.
% - Initial condition X0(3) changed to 0 from 0.002827.
%03/12
% - Rubber graduation spring force equation changed from quadratic to two separate
%   linear, case depedent equations.
%02/17
% - Spring force polynomial functions corrected such that dependent
%   variables are in newtons and independent variables are in meters.
% - Rubber graduation spring variable changed from cubic to quadratic
%   equation.
% - Replace linear rubber exhaust valve force equation e10 with non-linear
```

```
%   polynomial.
% - Replaced educated guess for q2 with steady-state value from trial with
%   valve in initial condition.
%02/16
% - O-ring frictions changed from sign() functions to atan() functions.
% - Orifice cross section area equations (Ai & Ae) corrected and enabled.
%02/15
% - q10_0 initial condition changed from .500 inches compression (+) to .08
%   inches clearance (-)
% - Changed initial condition q15_0 TO -9.13e-5 based on steady-state
%   result for q15 of first trial.
% - Effective areas of inlet seat and exhaust seat changed to case
%   dependent variables.
%02/13
% - Copy script from A6_2_state_der.m model; create A7_1 model.
% - Set derivative equations pdot30 and pdot 34 equal to zero.
% - Change nomenclature from R11_r to R32_r to match bond graph.
% - Change state derivative equation qdot33 to match A7_1 updates.
% - Change nomenclature from R21_r to R35_r to match bond graph.
% - Change state derivative equation qdot36 to match A7_1 updates.
% - Change state derivative equation qdot37 to match A7_1 updates.
% - Change state derivative equation qdot38 to match A7_1 updates.
%=========================================================================
%01/21
% - Archive A6_1 Model.
% - Minimized oscillating effects of fluid inertia by artificially
%   increasing pneumatic hose areas to unrealistically large numbers.
%01/20
% - Replaced linear spring models for efforts e15b and e10 (spring effect
%   of rubber coating on I/E valves) with experiementally determined
%   polynomial.
% - Replaced the linear expression (q2/C2_c) for force due to spring
%   compression with a non-linear function, e2.
% - Change to q38_0 = 1.0381e-07 from 7.5634e-05 to create steady state
%   condition e30_0 = pdot30 = 0.
%01/17
% - Redefined q15 to be displacement of the metal I/E valve poppet sructure
%   rather than the compression of the I/E valve poppet return spring.
%   Changed initial condition to match.
% - Split net spring force on poppet valve into e15_b and e15_c; e15_b being
%   the conditional spring force caused by contact of the inlet seat with the
%   poppet rubber.
% - Added limit for I/E valve body travel (q15).
%01/14
% - Multiplied effective spring rate estimates for ka & kb to 9X of kc
%   from 9X of kc
% - Changed initial condition of supply line fluid moment to 0 from
%   1.9834e4
```

```
%11/20
% - Added case dependency for e15.
% - Replace q15/C15_c in equation for pdot16 with e15.
% - Add bond graph-based names to initial conditions q10 and q15.
% - Added case dependency for e10.
% - Replace q10/C10_c with e10 in pdot16 and pdot9 eqs.
% - Change q37_0 initial condition to zero

%Parameter Definitions
%V21 = Delivery System Volume (in^3)
%V11 = Supply Volume in Reservoir Tank and Line (in^3)
%V37 = Fluid Volume in FBV Delivery Chamber (in^3)
%V38 = Fluid Volume in FBV Supply Chamber (in^3)
%C21 = Fluid Capacitance of Delivery Volume
%I11 = Fluid Inertia of Primary Supply Line
%c_air = Speed of Sound in Air
%Ru = Universal gas constant (kPa-m^3/(kgmol-K)
%Mair = Molar Mass of Air (moles)
%Rspec = Specific gas constant of air (bar-m^3/(kg-degK)
%rho0 = Density of air at reference pressure (1 atm)
%rho21 = Average density of air in primary delivery line
%rho31 = Average density of air in exhaust chamber
%l15c = Compression length of spring 15.c (m)
%l15c_0 = Pre-compression length of spring 15.c with 0 rubber deflection (in)
%h15b_0 = Undefelected height of rubber on I/E valve poppet (in)
%l21 = Length of primary delivery line (m)
%l31 = Length of exhaust chamber in valve (m)
%Impp = Inertia due to mass of primary piston (kg)
%Imie = Inertia due to mass of primary I/E valve (kg)
%Imrp = Inertia due to mass of relay piston (kg)
%A21 = Area of delivery line (in^2)
%A31 = Area of exhuast passage (in^2)
%P31 = Pressure of air in exhaust chamber (psig)
%P21 = Pressure of air in delivery line (psig)
%P0 = Pressure of Test Environment (psia)
%ka = Spring rate - Rubber Coating on Exhaust Valve
%kb = Spring rate - Rubber Coating on Inlet Valve
%kc = Spring rate - I/E Valve Spring (lb/in)
%kd = Spring rate - Rubber Graduation Spring (lb/in)
%ke = Spring rate - Primary Piston Return
%Ckc = 1/Spring rate of I/E valve spring (lbs/in)
%Ckb = 1/Spring rate of Rubber on Exhaust Valve
%Cka = 1/Spring rate of Rubber on Inlet Valve
%A1 = Net Effective Area on Inlet Side of I/E (m^2)
%A2 = Net Effective Area on Exhaust Side of Primary I/E (m^2)
%A3 = Net Effective Area on Primary Piston (m^2)
%D1 = Effective Diameter of Inlet Seat (in)
%D2 = Effective Diameter of Exhaust Seat (in)
```

```
%D3 = I/E Valve Body Diameter (in)
%D4 = Effective Primary Piston Diameter (in)
%D5 = Upper Body Supply Chamber Diameter (in)
%f3 = Friction - primary piston o-ring (lbs.)
%Ai = Inlet Orifice Size Ai(t) (inches)
%Ae = Exhaust Orifice Size (Ae(t)) (inches)
%b2 = O-Ring Friction of I/E Valve O-Ring (lbs.)
%b3 = O-Ring Friction of Primary Piston (lbs.)
%fluid11_i = Fluid Inertia of Primary Supply Line
%fluid21_i = Fluid Inertia of Primary Delivery Line
%C33 = Fluid Capacitance of Primary Supply System
%R11 = Flow Resistance in Supply Line
%R21 = Flow Resistance in Delivery Line
%u1 = Real Flow Input - Plunger Velocity (in/s)
%u2 = Real Effort Input - Primary Reservoir Pressure (psi)
%u3 = Substitute Flow Input - Resistance; Fluid Flow Through Inlet Valve
%u4 = Substitute Flow Input - Resistance; Fluid Flow Through Exhaust Valve
%u5 = Substitute Effort Input - Resistance; O-Ring Friction, I/E Valve Body
%u6 = Substitute Effort Input - Resistance; O-Ring Friction, Primary Piston
%ID11 = Nominal ID of Reservoir Supply Line (m)
%ID21 = Nominal ID of Valve Delivery Line (m)
%A11 = Cross Sectional Area of Supply Line (m)
%A21 = Cross Sectional Area of Delivery Line (m)
%C37 = Fluid Capacitance of Primary Delivery Volume in Valve Body
%C38 = Fluid Capacitance of Primary Supply Volume in Valve Body
%L4 = Height of Delivery Volume in Valve Body
%L5 = Height of Supply Volume in Valve Body
%mu = Coefficient of Shear Viscosity for Air Std. P & T (Pa-s)
%h = free thickness of rubber on top of I/E valve

%------------------------------------------------------------------------
% Parameters in USCS Units
%------------------------------------------------------------------------
V21 = 30; %Educated Guess
V11 = 300; %Educated Guess
T = 531.67; % DEG R - 72 DEG F for standard lab conditions
P0 = 14.696; %psia
kc = 8; %From Spring Drawing
%ka = 90*kc; %Educated Estimate
%kb = ka; %Educated Estimate
%kd = 707; %Based on similar product E-10 spring drawing
ke = 7.1; %From Spring Drawing
D1 = 1.031; %From Upper Body Drawing
D2 = .969; %From Primary Piston Drawing
D3 =.938; %From I/E Valve Drawing
D4 = 3.0; %From Upper Body Drawing
D5 = 1.46; %From Upper Body Casting Drawing
L4 = .25; %Educated Guess
```

```
L5 = 1.568-.850; %From Upper Body Drawing
l15c_0 = 1.1359; %From tolerance stack #8 and P/N 5001516
h15b_0 = .19+.0149; %From tolerance stack #8 (E and F)
b2 = 5; %Based on Random Guess
b3 = 5; %Based on Random Guess

%------------------------------------------------------------------------
% Conversion from USCS to Metric
%------------------------------------------------------------------------
V21 = V21*.0254^3; %Convert from in^3 to m^3
V11 = V11*.0254^3; %Convert from in^3 to m^3
T = T/1.8; %Convert from DEG R to K
P0 = P0*6894.75729; %Convert from psi to Pa
kc = kc*4.48/.0254; %Convert from Lbs/in to N/m
%ka = ka*4.48/.0254; %Convert from Lbs/in to N/m
%kb = kb*4.48/.0254; %Convert from Lbs/in to N/m
%kd = kd*4.48/.0254; %Convert from Lbs/in to N/m
ke = ke*4.48/.0254; %Convert from Lbs/in to N/m
D1 = D1*.0254; %Convert inches to meters
D2 = D2*.0254; %Convert inches to meters
D3 = D3*.0254; %Convert inches to meters
D4 = D4*.0254; %Convert inches to meters
D5 = D5*.0254; %Convert inches to meters
L4 = L4*.0254; %Convert inches to meters
L5 = L5*.0254; %Convert inches to meters
l15c_0 = l15c_0*.0254; %Convert inches to meters
h15b_0 = h15b_0*.0254; %Convert inches to meters
b2 = b2*4.48; %Convert lbs. to N
b3 = b3*4.48; %Convert lbs. to N

%------------------------------------------------------------------------
% Metric Parameters
%------------------------------------------------------------------------
c_air = 343; % m/s @20 DEG C and 1 atm
rho0 = 1.210; %kg/m^3
Impp = 0.1570; %Single measurement in lab (kg)
Imie = 0.0174; %Single measurement in lab (kg)
l11 = 5; %Based on educated engineerig assumption
l21 = 5; %Based on educated engineering assumption
ID11 = 0.01120; %SAEJ844 ID for 5/8 Nominal OD tubing
%ID21 = .00639; %SAEJ844 ID for 3/8 Nominal OD tubing
Ru = 8.314; %Tables and Figures
Mair = 28.97; %Table and Figures
mu = 1.8e-5; %KMR Appendix

%------------------------------------------------------------------------
% Derived Constants
%------------------------------------------------------------------------
```

```
%A11 = pi()*(ID11)^2/4; %Tubing Internal x-sectional area
%A21 = pi()*(ID21)^2/4; %Tubing Internal x-sectional area
V37 = D4^2*pi()*L4/4; %Rough Estimate: Measure Fluid Displacement Directly
V38 = (D5^2-D3^2)*pi()*L5/4; %Rough Estimate: Measure Fluid Displacement Directly
Rspec = Ru/Mair;
C21 = V21/(rho0*c_air^2); %Based on previous estimate for V21
C33 = V11/(rho0*c_air^2); %Based on previous estimate for V11
C37 = V37/(rho0*c_air^2); %Based on previous estimate for V37
C38 = V38/(rho0*c_air^2); %Based on previous estimate for V38
%Cka = 1/ka;
%Ckb = 1/kb;
%Ckd = 1/kd;
R11 = 128*mu*l11/ID11^4;
R21 = 128*mu*l21/ID11^4;
%Ckc = 1/kc;
%kbc = kb+kc;
%Ckbc = 1/kbc;
Cke = 1/ke;
%A1 = pi()/4*(D1^2-D3^2);
%A2 = pi()/4*(D1^2-D2^2);
A3 = pi()/4*(D4^2-D2^2);

%-----------------------------------------------------------------------
% Definition of States and Inputs
%-----------------------------------------------------------------------
x_names = {
'C10_state'; % q10 = Displacement of Poppet Rubber Under Exhaust Seat (m)
'C15_state'; % q15 = Displacement of Combined Inlet Spring Forces (m)
'C2_state'; % q2 = Displacement of Rubber Graduation Spring (m)
'C33_state'; % q33 = Fluid Displacement of Supply Line (m^3)
'C36_state'; % q36 = Fluid Displacement of Delivery Line (m^3)
'C37_state'; % q37 = Fluid Displacement of Delivery Chamber in Valve (m^3)
'C38_state'; % q38 = Fluid Displacement of Supply Chamber in Valve (m^3)
'C5_state'; % q5 = Displacement of Primary Piston Return Spring (m)
'I16_state'; % p16 = Momentum of Primary I/E Valve (kg.m/s)
'I30_state'; % p30 = Fluid Momentum of Supply Line
'I34_state'; % p34 = Fluid Momentum of Delivery Line
'I9_state'; % p9 = Momentum of Primary Piston (kg-m/s)
};


u_names = {
'u1_p.f'
    'u2_p.e.'
    'e4_p.e.'
    'e14_p.e'
    'f23_p.f.'
    'f29_p.f.'
```

```
};


%-------------------------------------------------------------------------
% Initial Conditions
%-------------------------------------------------------------------------
% Initial conditions are based on foot brake valve plunger travel = 0
% inches.  The primary piston and top of graduation spring are flush with
% the upper body machined surface.

q10_0 = -.08*.0254; %X0(1): Estimate of rubber exhaust compression stack (m)
q15_0 = -9.13e-5; %X0(2): Based on tolerance stack of valve (m)
q2_0 = 0.0; %X0(3): Rubber spring is initially not compressed (m)
q33_0 = .0321; %X0(4): Based on e33 = 135 psi (m^3)
q36_0 = 0; %X0(5): Delivery pressure is 0 psig before start of simulation (m^3)
q37_0 = 0; %X0(6): Delivery pressure is 0 psig before start of simulation (m^3)
q38_0 = 1.0381e-07; %X0(7): Such that pdot30_0 = 0 @ 135 psi supply P (m^3)
q5_0 = (3.66-.7370)*.0254; %X0(8): Based on master stack #6 and dwg 244453 (m)
p16_0 = 0; %X0(9): I/E valve velocity = 0 @ t=0.
p9_0 = 0; %X0(9): Primary Piston velocity = 0 @ t=0.

X0(1) = q10_0; %q10
X0(2) = q15_0; %q15
X0(3) = q2_0; %q2
X0(4) = q33_0; %q33
X0(5) = q36_0; %q36
X0(6) = q37_0; %q37
X0(7) = q38_0; %q38
X0(8) = q5_0; %q5
X0(9) = p16_0; %p16
X0(10) = p9_0; %p9


%-------------------------------------------------------------------------
% Read and Store the States
%-------------------------------------------------------------------------
q10 = X(1);

% Limit q15 to physically possible values
if X(2) < -h15b_0
    q15 = -h15b_0;
else
    q15 = X(2);
end

q2 = X(3);
q33 = X(4);
```

```
q36 = X(5);
q37 = X(6);
q38 = X(7);
q5 = X(8);
p16 = X(9);
p9 = X(10);

%-------------------------------------------------------------------------
% Read and Store the Inputs
%-------------------------------------------------------------------------
u1 = U(1);
u2 = U(2);

%-------------------------------------------------------------------------
% Time Dependent Derived Parameters
%-------------------------------------------------------------------------
P11 = u2;
e37 = q37/C37;
P21 = e37;
P31 = 0;
%rho11 = (P11+P0)/(1000*Rspec*T);
rho21 = (P21+P0)/(1000*Rspec*T);
%rho31 = P0/(1000*Rspec*T);
%I21 = rho21*l21/A21;
%I11 = rho11*l11/A11;


%-------------------------------------------------------------------------
% e15
%-------------------------------------------------------------------------
% e15 is the net spring force on the inlet valve metal and is the sum of a
% helical spring on the underside (e15_c) and a spring effect caused by the rubber
% on the top side (e15_b).  e15 is conditional based on whether the inlet seat is
% in contact (q15 <= 0) with the inlet seat or not.

l15_c = l15c_0 + q15;
e15_c = kc*(l15_c);
l15_b = q15;
e15_b = 1.2367e9*l15_b^2-3.8431e+005*l15_b+10.9299; %Experimental measurement (N)

if q15 > 0
    e15 = e15_c;
  else
    e15 = -e15_b + e15_c;
end

%-------------------------------------------------------------------------
% e10
```

```
%-------------------------------------------------------------------------
% e10 depends on exhaust seat contact with I/E valve rubber.  e11 is zero
% if the exhaust seat is "higher" than the top of the I/E valve rubber.
if q10 < 0
       e10 = 0;
    else
       e10 = 1.2367e9*q10^2-3.8431e+005*q10+10.9299;
end

%-------------------------------------------------------------------------
% e2 - Force due to compression (q2) of the non-linear rubber spring.
%-------------------------------------------------------------------------
%e2 = 7.3299e+13*q2^4-4.6580e+11*q2^3+8.3690e+08*q2^2-7.2749e+04*q2;
%using a1234 = [x3.^4, x3.^3, x3.^2, x3]\y3;
%e2 = 7.9858e13*q2^4-5.3681e11*q2^3+1.0964e9*q2^2-4.339e5*q2...
%+146.6042100; %using polyfit
if q2 < .003759
    e2 = (1.076e+003/.003759)*q2;
else
    e2 = ((1076-6278)/(.003759-.004806))*q2 - 1.760e+004;

end
%-------------------------------------------------------------------------
% Variable Substitutions for Linearization
%-------------------------------------------------------------------------

  I16_i = Imie;
  I9_i = Impp;
%  I30_i = I11;
%  I34_i = I21;
%  A2_r = A2;
  A3_r = A3;
%  A1_r = A1;
%  C10_c = Cka;
%  C15_c = Ckbc;
  C37_c = C37;
  C38_c = C38;
  C33_c = C33;
  R32_r = R11;
  C36_c = C21;
  R35_r = R21;
%  C2_c = Ckd;
  C5_c = Cke;

%-------------------------------------------------------------------------
% Modal Cases for Transformers
%-------------------------------------------------------------------------
if q15 > 0; %q15 > 0 => Inlet Seal Open | Apply
```

```
    A1_r = 0;
else %q15 < 0 => Inlet Seal Closed | Release or Lap
    A1_r = pi()/4*(D1^2-D3^2);
end

if q10 > 0; %q10 > 0 => Exhaust Seat Closed | Apply or Lap
    A2_r = pi()/4*(D1^2-D2^2);

%    A3_r = pi()/4*(D4^2-D2^2);
else %q10 < 0 => Exhaust Seat Open | Release
    A2_r = 0;
%    A3_r = pi()/4*(D4^2);
end
%--------------------------------------------------------------------------
% Calculate Fluid Flow Volume Through Inlet Orifice (f23)
%--------------------------------------------------------------------------

Ai = (pi()*D1)*q15; %Surface area of a cylinder (m^2)

if Ai > 0;
    Ai = Ai;
else
    Ai = 0;
end

f23 = Ai*sqrt((2/abs(rho21))*abs(P11-P21))*sign(P11-P21);

%--------------------------------------------------------------------------
% Calculate Fluid Flow Volume Through Exhaust Orifice (f29)
%--------------------------------------------------------------------------
%The exhaust orifice is modeled as the surface area of the side of a
%cylinder with height = abs(q10) and diameter = D2.  Contact or
%interference with the rubber exhaust valve sealing surface is represented
%by a positive value for q10.

Ae = (pi()*D2)*-q10; %Surface area of a cylinder (m^2)


if q10 < 0;
    f29 = Ae*sqrt((2/abs(rho21))*abs(P21-P31))*sign(P31-P21);
else
    f29 = 0;
end


%--------------------------------------------------------------------------
% Calculate O-Ring Friction (u5)
%--------------------------------------------------------------------------
```

```
f16 = p16/I16_i;
f14 = f16;
e14 = -(b2/1)*(2/pi())*atan(10*f14);

%-------------------------------------------------------------------------
% Calculate O-Ring Friction (u6)
%-------------------------------------------------------------------------
f9 = p9/I9_i;
f4 = f9;
e4 = -(b3/1)*(2/pi())*atan(10*f4);


%-------------------------------------------------------------------------
% State Derivatives
%-------------------------------------------------------------------------
qdot10 = p9/I9_i - p16/I16_i;
qdot15 = p16/I16_i;
qdot2 =  u1 - p9/I9_i;
qdot33 = (u2 - q33/C33_c - q38/C38_c)/R32_r;
qdot36 = (q37/C37_c - q36/C36_c)/R35_r;
qdot37 = f23 + f29 - (q37/C37_c - q36/C36_c)/R35_r - (A2_r*p16)/I16_i...
    + (A3_r*p9)/I9_i;
qdot38 = (u2 - q33/C33_c - q38/C38_c)/R32_r - f23 + (A1_r*p16)/I16_i;
qdot5 =  p9/I9_i;
pdot16 = e14 + e10 - e15 + (A2_r*q37)/C37_c - (A1_r*q38)/C38_c;
pdot9 =  e4 - e10 + e2 - q5/C5_c - (A3_r*q37)/C37_c;

%-------------------------------------------------------------------------
% Output
%-------------------------------------------------------------------------
xdot = [qdot10; qdot15; qdot2; qdot33; qdot36; qdot37; qdot38; qdot5;...
    pdot16; pdot9];


e36 = q36/C36_c;
Y = e36/6894.75729; %Convert from Pa to psi

monitor = e2;

out=[xdot;Y;monitor];
end
```